

**AN INVESTIGATION INTO THE EFFECT OF INCREASING THE NUMBER OF
COILS ENERGIZED PER PHASE ON THE EFFICIENCY OF SHORT-RANGE
SENSORLESS LINEAR TUBULAR MOTORS**

Author: Derek Lam
Date: February 3, 2015

ABSTRACT (295 words)

By eliminating the need for gearbox conversion systems, linear motors have significant advantages in terms of efficiency and compactness over their rotational counterparts in linear actuation applications. However, linear motors have the unique restriction of having a limited range of operation that rotational motors do not. As a result, these motors are far more often employed in short/finite-range applications rather than long-range or continuous ones, like in automobiles.

While extensive research has been conducted on optimizing the commutation sequence of continuous-motion rotational motors to maximize efficiency at high-speed operating points, far less has been done to optimize motors operating at the transitory speeds experienced in finite-range applications. The efficiency of finite-range linear motors changes dramatically over the course of their operation, partially determined by the way they are commutated. The purpose of this essay is to evaluate the effect energizing more coils per phase has on the “tubular” linear motor design specifically.

This effect was identified experimentally. A sensorless tubular linear motor was constructed and driven by three different commutation sequences. The position of theforcer, the electrical current and the potential difference across the motor were measured simultaneously as the motor traversed the range of its motion. Output and input power were calculated and the quotients of their maxima (power efficiency) and their integrals with respect to time (energy efficiency) were used to determine the overall efficiency of the sequence.

The data strongly support the hypothesis that sequences with more coils energized per phase are more efficient. The three-coil-per-phase sequence proved to be more efficient in both aspects than both the two- and one-coil-per-phase sequences. Nonetheless, some of the data was somewhat unreliable and prompts the search for a better method.

TABLE OF CONTENTS

| | |
|---|----|
| <u>Abstract</u> | i |
| 1.0: <u>Introduction</u> | 2 |
| 2.0: <u>Conceptualizing a linear motor</u> | 3 |
| 3.0: <u>Specifications</u> | 5 |
| 3.1: Physical Specifications | 5 |
| 3.2: Basic Circuit Specifications | 6 |
| 4.0: <u>Considerations for motor control</u> | 6 |
| 4.1: Source of spatial feedback | 6 |
| 4.2: Waveform type | 7 |
| 4.3: Sampling rate | 8 |
| 5.0: <u>Independent variable: Commutation Sequences</u> | 9 |
| 6.0: <u>Experimental Setup</u> | 10 |
| 6.1: Materials for experiment | 12 |
| 6.1: Equipment setup | 12 |
| 7.0: <u>Procedure</u> | 14 |
| 8.0: <u>Raw Data</u> | 14 |
| 8.1: Position, Velocity and Acceleration | 14 |
| 8.2: Current and Potential Difference | 17 |
| 9.0: <u>Calculations</u> | 20 |
| 8.1: Efficiency over time | 21 |
| 10.0: <u>Comparisons and Conclusions</u> | 23 |
| 10.1: Comparison of efficiencies of each sequence | 23 |
| 10.2: Conclusion | 25 |
| 11.0: <u>Possible Improvements</u> | 28 |
| 12.0: <u>Bibliography</u> | 29 |
| | |
| <u>Appendix 1</u> | 30 |
| <u>Appendix 2</u> | 31 |
| <u>Appendix 3</u> | 41 |
| <u>Appendix 4</u> | 43 |
| <u>Appendix 5</u> | 47 |

1.0: Introduction

The 21st century marks the beginning of society's uncanny addiction to some new applications of linear motion. A prominent example is the advent of 3D printers; there is an explosion of startups selling a veritable plethora of variations on this concept.

In order to function, most current 3D printers map models in Cartesian 3D (x,y,z) space, and move the extruder linearly along each axis to arrive at the desired point in space. The convenience of the Cartesian system is the intuitive nature of moving linearly in Cartesian space.

In most designs, rotational motors are used as they are more commonplace in the market. Yet, with ubiquity comes inefficiency in specialized situations. Adapting these types of motors to work in a linear application always requires some kind of conversion mechanism to convert the rotational motion into linear motion, which introduces complication, inefficiency and rapid wear. The intuitive solution is instead to use specialized *linear* motors, whose motion does not require mechanical conversion to actuate linearly. When considering the efficiency of their operation, however, one must consider the way their coils are commutated: that is, the sequence and waveform of the current sent through the coils. As much of the research into linear motors has gone into improving their positioning abilities, little research has been conducted on the effects the way they are commutated has on their efficiency. This essay attempts to fill some of this gap by investigating the role of the numerosity of coils energized per phase in determining the efficiency of the motor.

Research Question: Are commutation sequences that energize more coils per phase more efficient for linear motors moving over short distances than those that energize fewer?

The importance and unknown of this question stems from the fact that linear motors have a limited range of operation. Efficiency is not uniform throughout a motor's operation, but instead depends on the motor's speed. Because rotational motors have no limit to the distance their rotors can travel, these motors can attain any speed within between 0 and the maximum speed for a given output torque, including the speed at which it is operating more efficiently. For induction motors, this speed is often just greater than 60-90% synchronous speed (breakdown torque)^[1]. Conversely, linear motors are often restricted to a speed far below this speed due to their finite range of operation. This implies that the most efficient way to drive a linear motor is not necessarily the

¹ Computing the Lumped Parameters of Induction Machine Models. (n.d.). Retrieved October 16, 2014, from <http://www.infolytica.com/en/applications/ex0173/>

most efficient sequence for the equivalent rotational motor operating at far higher speeds, but could rather be the sequence whose efficiency increases *the fastest*.

2.0: Conceptualizing a linear motor

The easiest way to understand a linear motor is to imagine a straight row of magnets parallel to a straight row of coils: an unraveled rotational motor. When current flows through a coil, the resulting magnetic field acts like a permanent magnet magnetized orthogonally to the coil's area. This is known as *energizing* the coil. The polarity of this "magnet" depends on the direction that current is sent through the coil. If the conventional current at the top of the coil approached the observer while it recessed at the bottom (top, Fig 1), the magnetic field inside the coil will point to one's right². If the predominant direction of the coil's magnetic field is in the same direction as that of a magnet's, they will attract and accelerate towards each other. If, at the moment the magnet reaches this coil, current is redirected to another coil further along the magnet's path, the magnet will continue to accelerate in that direction. This is known as commutation. Fig 1 demonstrates a simplified version of the linear motor commutation used in the experiment which shows how theforcer experiences a rightward force at each phase.

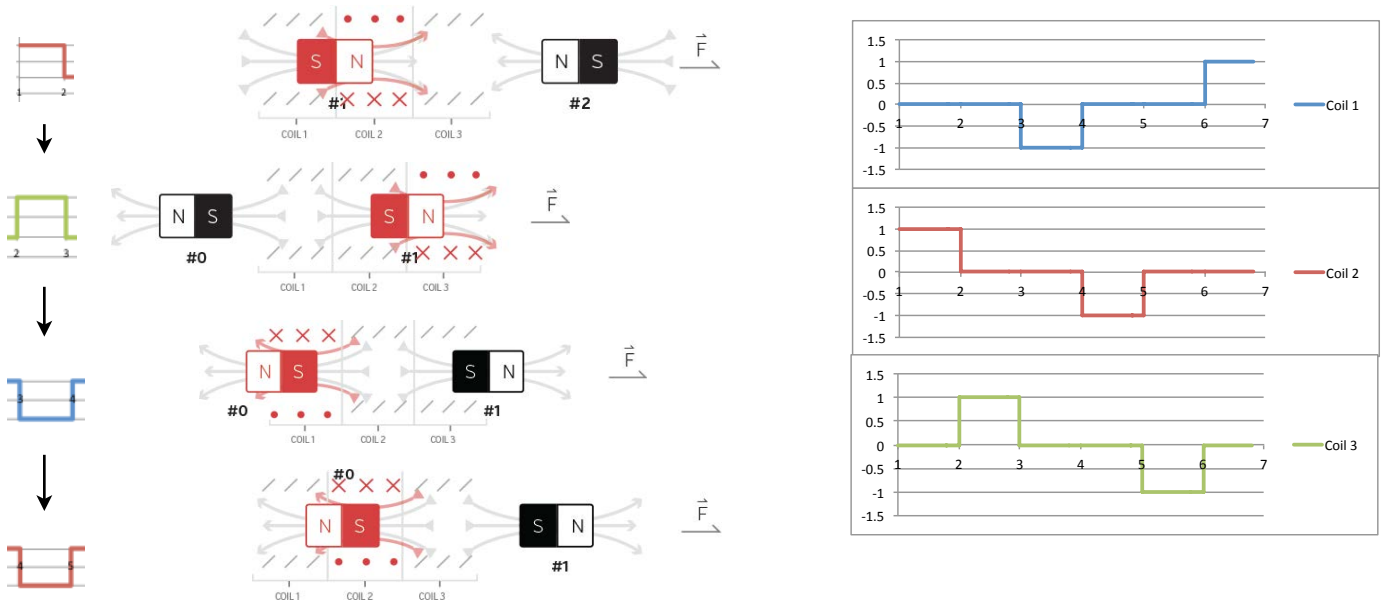


Fig 1: Cross-section of half of the stator as viewed from orthogonal to the stator's axis. Grey arrows represent magnetic field of magnet, red arrows represent magnetic field of stator. The graph on the right represents the sequence to energize the coils on the left.

² Halliday, David, and Robert Resnick. "Chapter 31: Ampere's Law." Fundamentals of Physics. II ed. Vol. I. United States: John Wiley & Sons, 1981. 564. Print. Extended Version.

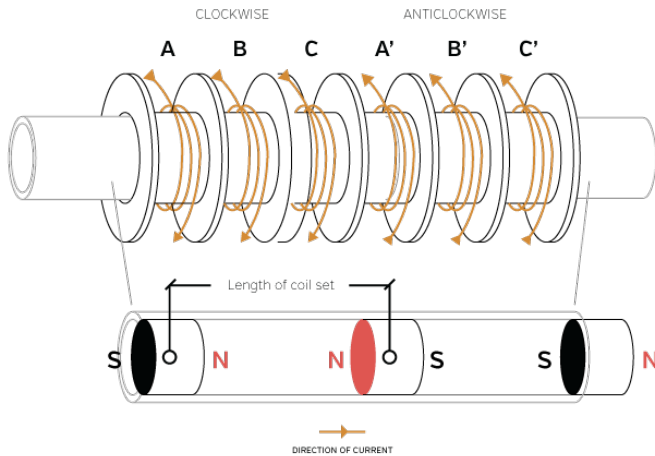
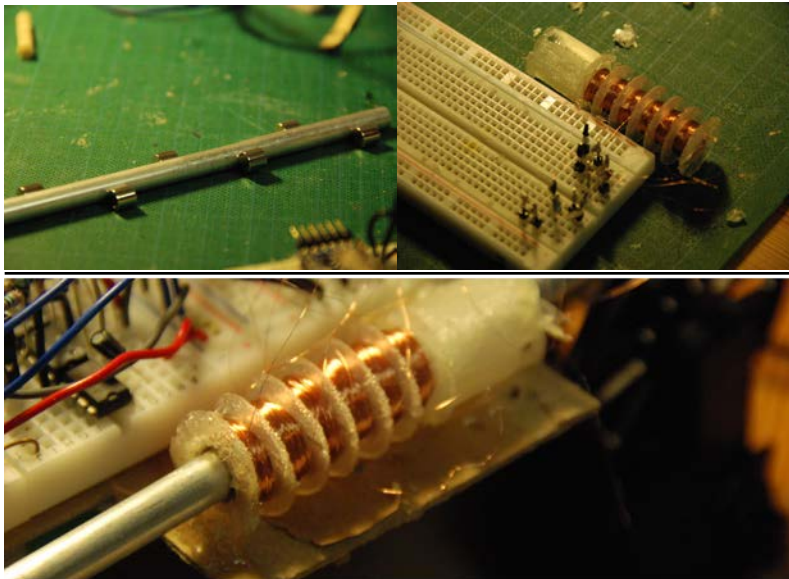


Fig 2. Simplified design of the 3-phase tubular linear motor with two sets of coils (primed and unprimed): stator (top) and cross-section of forcer showing embedded magnets (bottom). Unprimed coils are electrically connected to their primed equivalents.



Figures 3, 4 & 5: (clockwise from top left) The forcer used in the experiment, with magnets outside indicating the position and polarity of the magnets within; the 3D printed stator, fully wound and connected to a breadboard; the motor assembled.

The type of linear motor chosen for investigation is known as a tubular linear motor. It consists of a series of coils wrapped around a hollow, non-magnetic tube, known as the stator (top Fig. 2; white, plastic object in Fig. 4 & 5), and a rod embedded with evenly-spaced magnets, known as the forcer (bottom Fig. 2; metal rod in Fig. 3 & 5). The specific one constructed for the experiment consists of three *pairs* of oppositely-wound coils that are electrically connected such one cannot send current through one without sending current in the *opposite direction* through the other (e.g. A vs. A', Fig 2)

3.0: Specifications

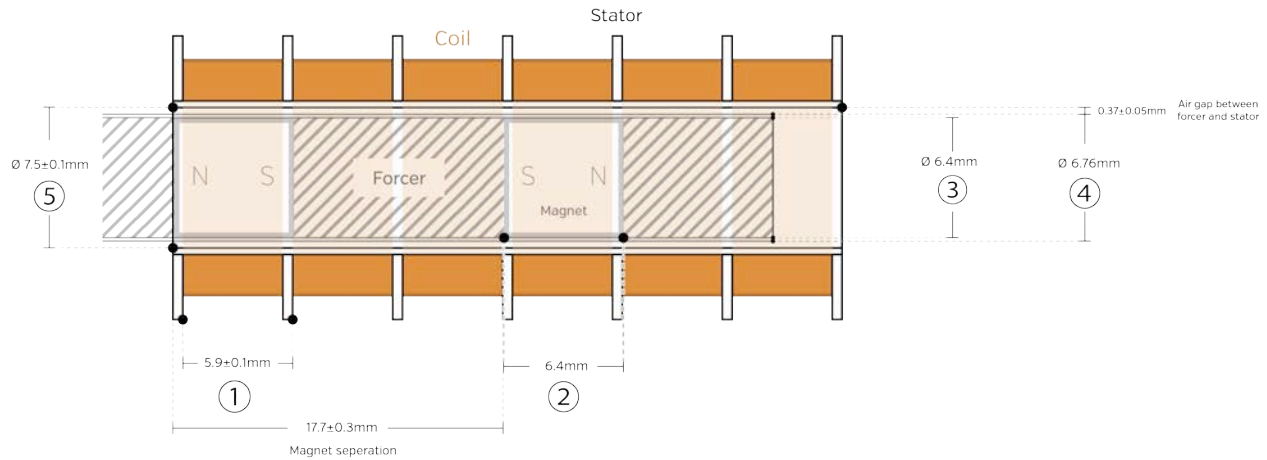


Fig 6. Cross section of motor viewed orthogonal to axis; includes both stator (outside) and forcer (inside). Lengths of crucial components are shown (see table 1).

3.1: Physical specifications:

Table 1: Design variables

| ① | ② | ③ | Shape of magnet | Direction of magnetization | Orientation of magnets |
|--|---|---|--------------------------------------|--|---|
| Motor pitch* | Length of magnet along axis of magnetization | Diameter of magnet | | | |
| $5.9 \pm 0.1 \text{ mm}$ | 6.4 mm | $\text{Ø} 6.4 \text{ mm}$ | Cylindrical | Axial | Alternating NS-SN-NS... |
| ③ | ④ | ⑤ | Number of magnets embedded in forcer | Effective range of operation*‡ (2 magnets in stator) | Maximum range of operation*‡ (1 magnet in stator) |
| Interior diameter of forcer enclosure | Exterior diameter of forcer enclosure | Interior diameter of stator scaffold model | | | |
| $\text{Ø} 6.4 \text{ mm}$ | $\text{Ø} 6.76 \text{ mm}$ | $\text{Ø} 8.436 \text{ mm}$ | 9 | $148.3.0 \pm 0.6 \text{ mm}$ | $166.0 \pm 0.6 \text{ mm}$ |
| Mass of forcer | | | | | |
| $28.063 \pm 0.001 \text{ g}$ | | | | | |

* Measured using a pair of calipers

‡ The effective range of operation was determined by measuring the distance between the first and last magnet ($154.2 \text{ mm} \pm 1 \text{ mm}$), and subtracting 1/3 the length of a coil set, or the pitch of the motor ($5.9 \pm 0.1 \text{ mm}$). The maximum range of operation was determined by taking the effective range and adding the length of a coil set, or three times the pitch of the motor ($17.7 \pm 0.3 \text{ mm}$). The maximum range of operation is defined as the range of the motor if it operates with two magnets in the stator at the beginning and ends with one; while the effective range is defined as the range of the motor that operates with two magnets in the stator at all times.

Table 2: Materials

| Forcer enclosure | Stator scaffold | Coil | Magnet |
|------------------|-----------------|-------------------|--------------------------|
| Aluminum | PLA | 36AWG copper wire | N40 Neodymium-iron-boron |

3.2: Basic circuit specifications *(See Appendix 2 for full details about the circuit):*

Table 3: Major circuit components

| Source EMF | Microcontroller & ADC | Switch | Feedback amplifiers |
|-------------------------------------|---|---------------|---------------------|
| 7.4V 2S 1000mAh Lithium Ion battery | Arduino Pro Mini 5V 16MHz [9600Hz built-in ADC] | L298 H-Bridge | L412 & L411 op amps |

4.0: Considerations for motor control

To isolate the effect coil numerosity has on efficiency, decisions were made to standardize the rest of the variables for all of the tests.

4.1: Source of spatial feedback: sensorless (“back” EMF)

To know which coil to energize when, it is useful to know the position of the forcer with respect to the stator. Most tubular motor technologies obtain very accurate position data and hence position the forcer with impressive precision. Attaining these results, however, often requires the use of bulky external sensors like linear-variable-differential transformer-[3], encoder-[4] [5] or hall-sensor-based[6] feedback systems, which hinders their ability to be used in compact applications. It is, alternatively, possible to actuate a linear tubular motor while forgoing external sensors.

As a current applies force to a magnet in a coil, so too does a moving magnet induce a current within a coil. As the forcer moves within the stator, the magnets embedded in

³ Murphy, Bryan C., and Won J. Kim. "Development of a Novel Direct-Drive Tubular Linear Brushless Permanent Magnet Motor" *International Journal of Control, Automation and Systems* 2.3 (2004): 283. IJCAS. Web. 2 Apr. 2014. <http://www.ijcas.org/admin/paper/files/IJCAS_v2_n3_pp279-288.pdf>.

⁴ Kim, Won J., M. T. Berhan, D. L. Trumper, and J. H. Lang. "Analysis and Implementation of a Tubular Linear Motor with Halbach Magnet Array." *Analysis and Implementation of a Tubular Motor with Halbach Magnet Array* (1996): 476. IEEE. Web. 29 Apr. 2014. <http://ieeexplore.ieee.org/xpl/login.jsp?tp=&arnumber=557069&url=http%3A%2F%2Fieeexplore.ieee.org%2Fxppls%2Fabs_all.jsp%3Farnumber%3D557069>.

⁵ Hygenic Servotube Actuator. Dunker Motoren Linear Systems, n.d. Web. 11 Apr. 2014. <http://www.dunkermotoren.com/data/linearsysteme/downloads/DS01102_EN.pdf>.

⁶ Ibid.

the forcer induces current in the stator's coils, the magnitude of which relates to both the forcer's velocity and displacement. Lenz's Law implies that the direction of the induced current caused by a moving magnet (or any change in flux for that matter) creates a magnetic field that applies a force on the magnet opposite to its motion⁷. Intuitively, sending current in the opposite direction of the induced current will apply a force on the magnet *in the direction of its motion*, so by the signage of the current alone, the motor can cause the rod to accelerate reliably without external sensors. (see Appendix 2 for full explanation and theory)

While the viability of this technique is disputed for positioning purposes^{8 9}, for the purposes of actuation, this technique proved to be more than sufficiently accurate.

4.2: Waveform type: rectangular (3-state)

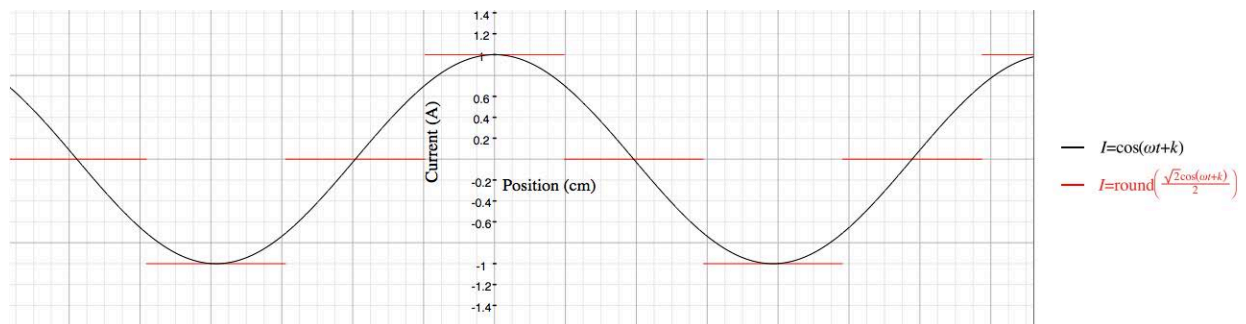


Fig 7. A graph plotting current to one coil vs. position of the forcer, outlining the difference between a sinusoidal AC waveform (black) and a rectangular waveform (red)

⁷ Halliday, David, and Robert Resnick. "Chapter 31: Ampere's Law." Fundamentals of Physics. II ed. Vol. I. United States: John Wiley & Sons, 1981. 577. Print. Extended Version.

⁸ Holtz, J., "Sensorless Control of Induction Machines—With or Without Signal Injection?", IEEE Transactions on Industrial Electronics, Volume 53, Issue 1, Feb. 2006, pp. 7 – 30.

⁹ Silva, C., Asher, G.M. and Sumner, M., "Hybrid rotor position observer for wide speed ranger Sensorless PM motor drives including zero speed", IEEE Transactions on Industry Electronics, Vol. 53, N° 2, April 2006.

External literature by F. Cupertino et al.^[10], B. C. Murphy^[11] and W. J. Kim^[12] et al. suggests that the conventional waveform used to drive linear motors is a 3-phase sinusoidal waveform (Fig. 7), with each coil offset by $\frac{2}{3}\pi$. However, to do so requires

three things:

- 1) precise knowledge of theforcer's position or angular frequency at all times,
- 2) a sufficiently fast microcontroller (e.g. the 250MHz TMS320FS240 chip used in Murphy's design) to generate the PWM signals which are then converted to sinusoidal waves via:
- 3) some filtering circuit; e.g. as mentioned explicitly in "Development of a Novel Direct-Drive Tubular Linear Brushless Permanent Magnet Motor": PWM amplifiers.

While not impossible to drive the motor with sinusoidal waveforms in a sensorless design, achieving any of these greatly increases the cost of the apparatus and the complexity of the calculations and circuit, not to mention a filter circuit introducing unwanted electrical inefficiency.

Instead of analogue output, the motor controller drove the coils into one of three discrete states: positive current, negative current and high-impedance at high frequency. The state of any given coil at any time was based on the nuances of the sequence tested, which themselves were based on the back EMF readings from the coils. Despite the superficial similarity to PWM and DAC systems, the two techniques differ in purpose. While PWM creates an equivalent analogue potential difference over a period of time magnitudes greater than the wave period, the former commutation schema focuses on the *discrete* state of coils at the microsecond timescale with no direct regard for the equivalent potential difference over large timescales.

¹⁰ Cupertino, Francesco, Paolo Giangrande, Gianmario Pellegrino, and Luigi Salvatore. "End Effects in Linear Tubular Motors and Compensated Position Sensorless Control Based on Pulsating Voltage Injection." IEEE58.2 (2011): 3. IEEE. Web. 30 Apr. 2014.

¹¹ Murphy, Bryan C., and Won J. Kim. "Development of a Novel Direct-Drive Tubular Linear Brushless Permanent Magnet Motor" International Journal of Control, Automation and Systems 2.3 (2004): 283. IJCAS. Web. 2 Apr. 2014.

¹² Kim, Won J., M. T. Berhan, D. L. Trumper, and J. H. Lang. "Analysis and Implementation of a Tubular Linear Motor with Halbach Magnet Array." Analysis and Implementation of a Tubular Motor with Halbach Magnet Array (1996): 476. IEEE. Web. 29 Apr. 2014.

It is of note that the resulting waveform is rectangular. While in positioning applications, using such a waveform is far from ideal in terms of step response^[13], in terms of linear actuation it comes at little expense to efficiency due to the proportionality of applied force to current^[14].

4.3: Sampling rate:

The coils need to be disengaged to measure back EMF (Appendix 2); as a result, the sampling rate directly determines the duty cycle of the motor, and hence affects the force the forcer experiences. Intuitively, the lowest possible sampling rate would yield largest force and hence the largest ratio of applied force to friction. However, if the sampling rate is too low, the commutation of the coils is inaccurate, which is detrimental to efficiency. As a result, a range of sampling periods ($\{560\mu\text{s}, 760\mu\text{s}, 960\mu\text{s}, 1160\mu\text{s}, 1360\mu\text{s}\}$) was tested, and the most efficient for each commutation sequence was used for comparison.

5.0: Independent Variable: Commutation Sequences

All of the sequences rely on specific properties of electromagnetic induction: namely that the induced potential difference is a function of velocity and displacement (*see Appendix 2 for more details*).

Each sequence begins by energizing one linked pair of coils to align the forcer. Then, for a few (10) milliseconds, three coils are energized to initially push the forcer in the desired direction, marking the beginning of the motor's operation. From there, the forcer is accelerated by positive feedback. Every few hundred microseconds, the microcontroller will stop all current to the coils and will measure the induced potential difference across each coil. The signage and *relative* magnitude of the induced potential difference can be used to determine the configuration of coils energized.

- 1) The three-coil sequence energizes all three coils per phase. It measures the direction of current from each coil and drives current through *all coils* in the opposite direction. As a result, while not being sampled, all coils are energized.

¹³ Murphy, Bryan C. "DESIGN AND CONSTRUCTION OF A PRECISION TUBULAR LINEAR MOTOR AND CONTROLLER." (2003): 68. Office of Graduate Studies of Texas A&M University. Web. <<http://repository.tamu.edu/bitstream/handle/1969.1/101/etd-tamu-2003A-2003032713-murp-1.pdf?sequence=1>>.

¹⁴ Robertson, Will, Ben Cazzolato, and Anthony Zander. "Axial Force between a Thick Coil and a Cylindrical Permanent Magnet: Optimising the Geometry of an Electromagnetic Actuator." IEEE 48.9 (2012): 3. IEEE. Web. 4 May 2014. <<http://personal.mecheng.adelaide.edu.au/will.robertson/research/2012-magcoil.pdf>>.

- 2) The two-coil sequence energizes two coils per phase: those with most negative and the most positive induced currents in the opposite direction to their induced currents. Assuming all coils are identical, energizing these coils maximizes applied force as the the effect of the resulting magnetic field will be the strongest on the magnets (*see Appendix 2 for more details*).
- 3) The single-coil sequence energizes the coil with the largest absolute induced potential difference in the opposite direction to its induced current. The logic follows the same as that of the two-coil sequence.

6.0: Experimental Setup

The goal of this experiment is to compare the power output of different commutation sequences. As such, a quantitative quality that applies to all mechanical systems regardless of the type of power input or the method of force propagation had to be employed. Efficiency is a metric that fits these criteria, and in the experiment it is

determined two ways: using power to find the efficiency at any point in time – $\eta = \frac{P_{out}}{P_{in}}$ –

and using energy to find the efficiency of the motor throughout its range: $\eta = \frac{E_{out}}{E_{in}}$. Power

efficiency is more convenient to use to illustrate trends, so in this essay, “efficiency” refers to power efficiency unless an explicit reference to “energy” efficiency is made.

Since the input energy is electrical, the input power of the motor is defined by $P = VI$.

Assuming the current consumed by the auxiliary electronics is negligible (*see Appendix 3 for details*), it is assumed that the current from the battery is equal to the current consumed by the coils and the drive circuit.

The output power for this setup was computed by measuring the change in total energy

over time: $P = \frac{dE_{tot}}{dt}$. If the forcer is driven horizontal to the ground, it can be assumed

that the change in energy is purely kinetic.

Kinetic energy is described by the relation $E_K = \frac{mv^2}{2}$. The change in kinetic energy over time can be expressed in terms of velocity and acceleration, shown in the following derivation:

$$P = \frac{dE_K}{dt} = \frac{d\left(\frac{mv^2}{2}\right)}{dt}$$

$$P = \frac{m}{2} \left(2v \frac{dv}{dt}\right)$$

$$P = mva$$

To measure the velocity and acceleration of the forcer over time, a Vernier Go!Motion sonar motion sensor was used. Positioned approximately 50cm away from the motor at the start of each trial, the motion sensor tracked the position of the forcer as it recessed from it and traversed the range of its motion.

To measure the potential difference across the battery, a potential divider comprised of two $2K\Omega \pm 1\%$ resistors was connected in parallel to the circuit, and the potential difference across the low-end resistor was recorded.

To measure current, a $0.4\Omega \pm 0.3\%$ ammeter shunt resistor was placed in series with the circuit, and the potential difference across the resistor was measured with the built-in 10-bit^[15] 9.6kHz^[16] ADC on the Arduino Pro Mini. This value was then divided by the resistance of the shunt.^[17]

¹⁵ "8-bit AVR® Microcontroller with 4/8/16/32K Bytes In-System Programmable Flash." ATMEL (n.d.): 250. Web. 2 May 2014. <<http://www.atmel.com/Images/doc8161.pdf>>.

¹⁶ Ibid. p. 264

¹⁷ The resistance values were selected carefully to yield usable results while having negligible influence on the circuit. From data gathered from a multimeter, the current through the circuit while the motor was running was on the order of 10^{-1} A, and the potential difference across the source was between 7-8V. Applying Ohm's law, we can deduce that, while the motor was running, the input impedance of the circuit was on the order of 10^1 - $10^2\Omega$. The 0.4Ω shunt had little contribution to the total resistance of the circuit, having a resistance a magnitude or two lower than the rest of it. In addition, the 1.5-2mA flowing through the potential divider is two magnitudes lower than the current measured through the motor, making it equally negligible to the circuit's operation.

6.1: Materials for experiment:

Table 4. Equipment list of materials necessary specifically to run the experiment.

| Measurement | | Structural Support |
|---|----------------------------|---|
| Electrical | Motion | |
| Arduino Pro Mini – 5V 16MHz, 10-bit 9.6kHz ADC | Vernier Go!Motion detector | 2x PASCO Super Pulley (to reduce friction) |
| 0.4 Ω ±3% 25W shunt resistor | | Cardboard boxes |
| 2x 2K Ω ±1% precision resistors | | |
| Oscilloscope (for debugging) | | |

6.2: Equipment Setup

Figures 8-12 outline macroscopic and specific aspects of the equipment setup graphically.

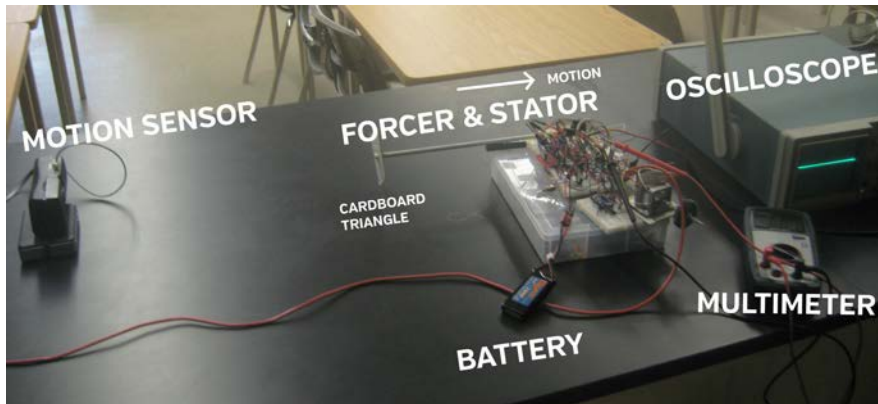


Fig 8. The overall setup of the experiment. The motor moves to the right, and its position is recorded by the ultrasonic motion sensor in the leftmost part of the image.

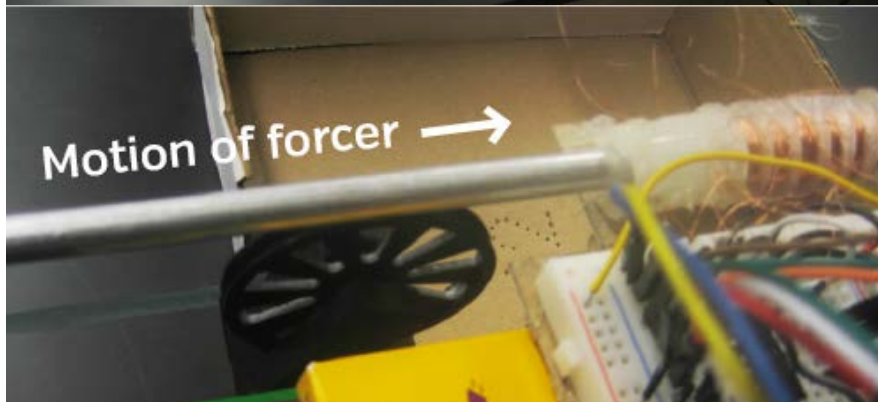


Fig 9. A PASCO low-friction Super Pulley (black wheel in center-left) supporting the weight of the forcer



Fig 10. The motion detector (foreground, left) pointed at the back of the forcer (background, white triangle). The forcer recesses from the sensor (goes into the page).

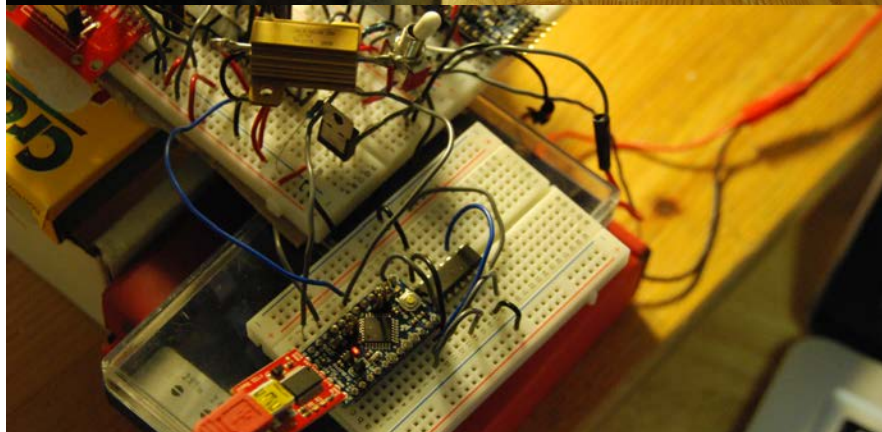


Fig 11. The ammeter and voltmeter for the circuit: an Arduino Pro Mini (center left, blue chip with red light) and the shunt resistor (top left, golden box) are shown. The precision resistors are too small to be seen.

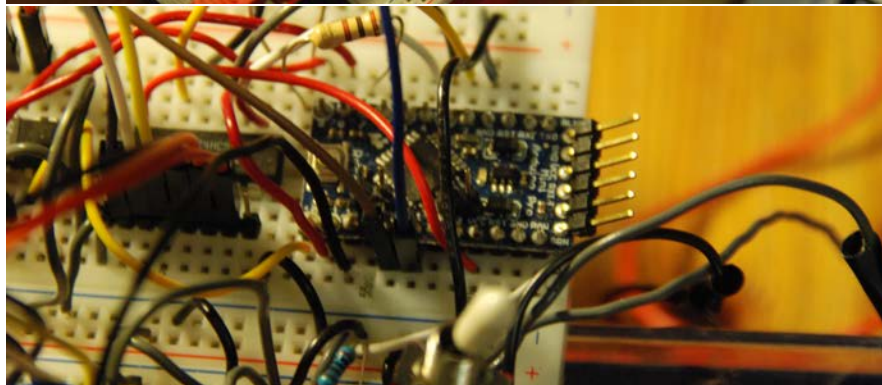


Fig 12. The processor: this Arduino commutates the current to the motor.

7.0: Procedure

Once the equipment is set up as shown in Figs. 8-12:

1. Upload desired commutation sequence to motor controller.
2. Connect measurement Arduino and Go!Motion detector to computer.
3. Prepare serial recording script to record current and voltage data; prepare Logger Pro to record position data
4. Press “RESET” pushbutton switch on motor controller.
5. Flip main power switch to “ON”
6. Within the next five seconds (delay set in code):
 - a. Ensure the forcer is in the proper starting position,
 - b. Run the serial recording script,
 - c. Begin recording position on Logger Pro.
7. Wait until the forcer has come to a full stop after the motor finishes running.
8. Within the next second:
 - a. Stop recording position on Logger Pro
 - b. Terminate the serial recording script
 - c. Flip the main power switch to “OFF”
9. Repeat from step 2. for more trials, or:
10. Change the sampling period in code and repeat from step 1, or:
11. Switch to another commutation sequence and repeat from step 1.

8.0: Raw Data

8.1: Position, velocity and acceleration

Table 5. Sample data table showing position, velocity and acceleration of the forcer vs. time while the forcer is moving. Note: the maximum range of the motor is 166.0mm.

| Time (t/s) | Position (d/m \pm 0.001m) | Velocity (v/m \cdot s ⁻¹) | Acceleration (v/m \cdot s ⁻²) |
|------------|-----------------------------|---|---|
| 1.16 | 0.505 \pm 0.001 | 0.017 \pm 0.000067 | 2.372 \pm 0.0024 |
| 1.18 | 0.505 \pm 0.001 | 0.076 \pm 0.0003 | 4.991 \pm 0.0066 |
| 1.2 | 0.507 \pm 0.001 | 0.21 \pm 0.00082 | 7.95 \pm 0.0059 |
| 1.22 | 0.512 \pm 0.001 | 0.411 \pm 0.0016 | 9.979 \pm 0.0063 |
| 1.24 | 0.523 \pm 0.001 | 0.634 \pm 0.0024 | 10.616 \pm 0.0069 |
| 1.26 | 0.538 \pm 0.001 | 0.856 \pm 0.0032 | 10.123 \pm 0.0078 |
| 1.28 | 0.558 \pm 0.001 | 1.043 \pm 0.0037 | 9.253 \pm 0.017 |
| 1.3 | 0.58 \pm 0.001 | 1.216 \pm 0.0042 | 8.492 \pm 0.0091 |
| 1.32 | 0.606 \pm 0.001 | 1.398 \pm 0.0046 | 6.566 \pm 0.0035 |
| 1.34 | 0.636 \pm 0.001 | 1.542 \pm 0.0049 | 1.536 \pm 0.00028 |
| 1.36 | 0.671 \pm 0.001 | 1.502 \pm 0.0045 | -5.937 \pm 0.0043 |
| 1.38 | 0.699 \pm 0.001 | 1.278 \pm 0.0037 | -12.488 \pm 0.0088 |

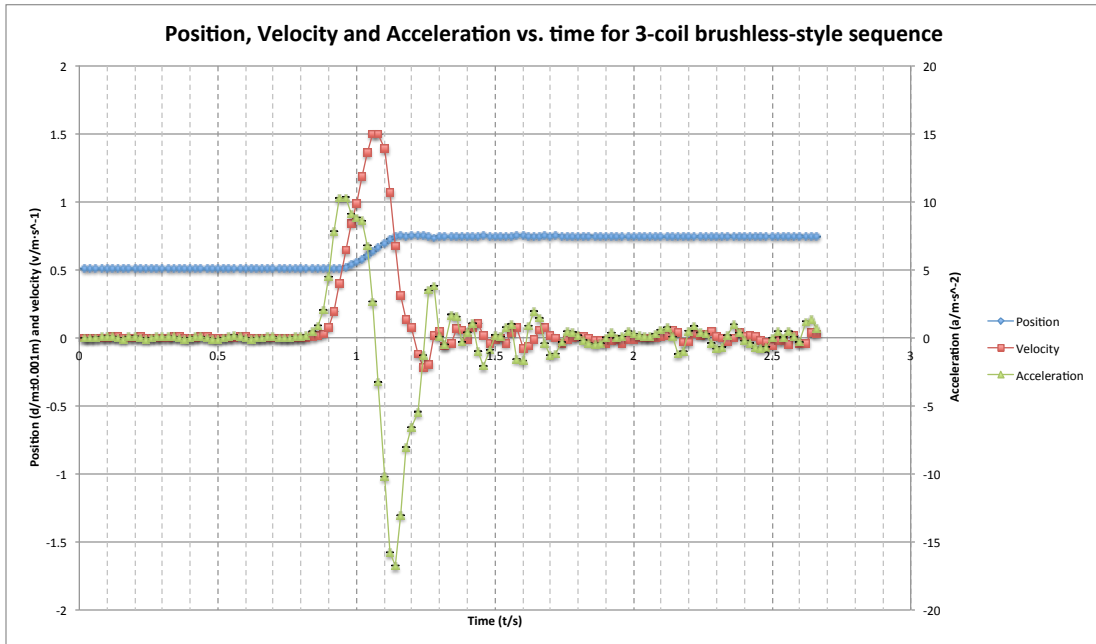


Fig 13. Graph showing position and velocity (left y-axis), and acceleration (right y-axis) of the forcer vs. time for the 3-coil sequence (feedback sampling period = $1160 \pm 20 \mu\text{s}$). Most of the error bars are too small to be seen.

The motion sensor only measures *position data* and calculates the first and second derivative to find velocity and acceleration respectively. According to their Tech Info Library, Logger Pro calculates derivatives of position by taking the weighted average of the slope of the points n ($n \bmod 2 = 1$) on either side of the point being evaluated^[20].

Generally, for the m th value of a function $y(t)$:

$$\frac{dy_m}{dt} = \frac{\left(\frac{y_{m-\lfloor \frac{n}{2} \rfloor} - y_{m+\lfloor \frac{n}{2} \rfloor}}{t_{m-\lfloor \frac{n}{2} \rfloor} - t_{m+\lfloor \frac{n}{2} \rfloor}} + 2 \frac{y_{m-\lfloor \frac{n}{2} \rfloor+1} - y_{m+\lfloor \frac{n}{2} \rfloor-1}}{t_{m-\lfloor \frac{n}{2} \rfloor+1} - t_{m+\lfloor \frac{n}{2} \rfloor-1}} + \dots + \left[\frac{n}{2} \right] \frac{y_{m-1} - y_{m+1}}{t_{m-1} - t_{m+1}} \right)}{\frac{\left[\frac{n}{2} \right] \left(\left[\frac{n}{2} \right] + 1 \right)}{2}} \quad (1)$$

The uncertainty of velocity and acceleration can quite easily be calculated solely from the uncertainties of the position measurements and velocity calculations respectively. From (1) (where $\epsilon(z)$ is percent uncertainty of the z th value of y):

²⁰ "How Does Logger Pro Calculate Velocity and Acceleration from Motion Detector Data?" Vernier Tech Info Library. Venier, 11 Jan. 2011. Web. 11 May 2014. <<http://www.vernier.com/til/1011/>>.

$$\Delta v(m) = \frac{(\varepsilon(m - \lfloor \frac{n}{2} \rfloor) + \varepsilon(m + \lfloor \frac{n}{2} \rfloor) + 2(\varepsilon(m - \lfloor \frac{n}{2} \rfloor + 1) + \varepsilon(m + \lfloor \frac{n}{2} \rfloor - 1)) + \dots + \lfloor \frac{n}{2} \rfloor (\varepsilon(m - 1) + \varepsilon(m + 1))) \cdot v(m)}{\frac{\lfloor \frac{n}{2} \rfloor (\lfloor \frac{n}{2} \rfloor + 1)}{2}} \quad (2)$$

Since it is known that $n=7$ (by default), (2) simplifies to:

$$\Delta v(m) = \left(\frac{\varepsilon(m - 3) + \varepsilon(m + 3)}{6} + \frac{(\varepsilon(m - 2) + \varepsilon(m + 2))}{3} + \frac{(\varepsilon(m - 1) + \varepsilon(m + 1))}{2} \right) \cdot v(m) \quad (3)$$

This was used to determine the error bars for Fig. 13 and the uncertainties in Table 5. However, since all of the results will be calculated by a computer, it was impractical to program a function so complex when the following approximation is quite sufficient:

Since the uncertainty of position is usually in the range of 0.14%-0.2%

($\frac{0.1}{75.0} < \varepsilon < \frac{0.1}{50.0}$), the percent uncertainty of velocity from (3) is usually ~0.17%.

Knowing this, the percent uncertainty of acceleration is also usually ~0.17%. To be generous, in the calculations, the uncertainty of v and a were assumed to be 0.5%.

8.2: Current and Potential Difference

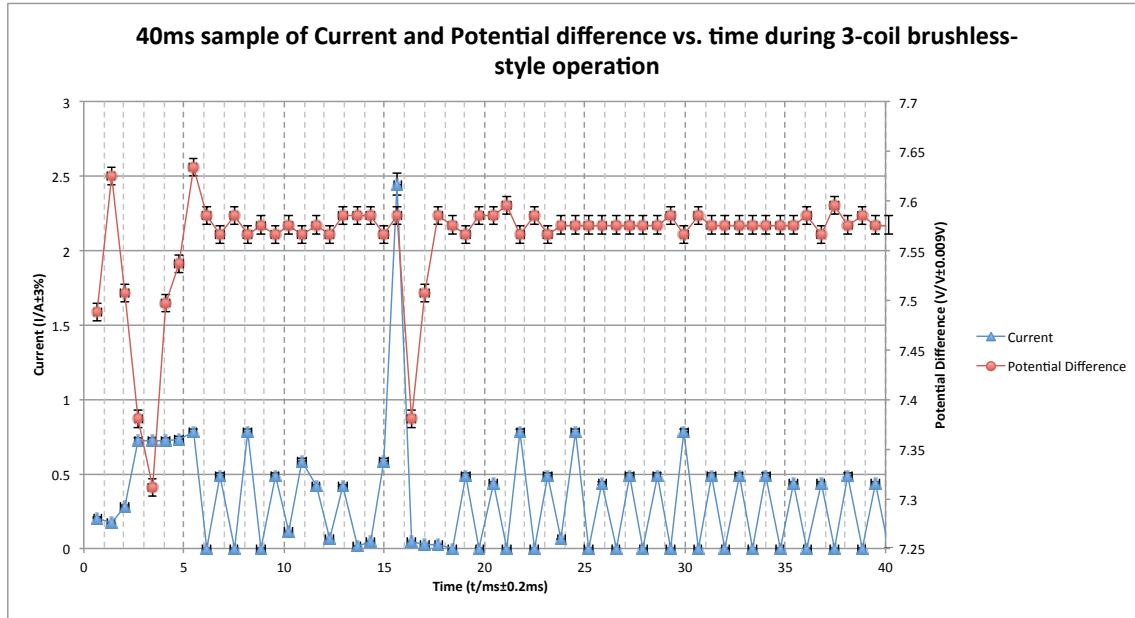


Fig 14. Graph showing the current through the circuit (blue, left y-axis) and the potential difference across the battery (red, right y-axis) while the motor is in operation (feedback sampling period = $1160 \pm 20 \mu\text{s}$). (see Appendix 4 for sample raw data)

It was determined experimentally^[21] that the sampling rate of the ammeter and voltmeter were $1468 \pm 1 \text{ Hz}$ ($681 \pm 1 \mu\text{s}$ sampling period).

The initial output of the ADC is a discrete 10-bit integer from 0-1023 that is mapped from the potential difference between 0-5V. To calculate the actual potential difference across the source, the reading was multiplied by $\frac{5}{1024}$ ^[22]. Because a potential divider was used to reduce the potential difference to the ADC when measuring the p.d. across the battery, the actual p.d. can be calculated with the potential divider formula:

$$V_m = \frac{Z_2}{V_{out}(Z_2 + Z_1)}$$

where $Z_1 = Z_2 = 2000 \Omega \pm 1\% = 2000 \pm 20 \Omega$.

²¹ A rectangular pulse was sent to one of the coils for $5.000060\text{s} \pm 8\mu\text{s}$, causing current to flow through the circuit. The amount of samples taken by the ammeter in those ~ 5 seconds was recorded and divided by $5.000060\text{s} \pm 8\mu\text{s}$ to yield the sampling rate.

²² "8-bit AVR® Microcontroller with 4/8/16/32K Bytes In-System Programmable Flash." ATMEL (n.d.): 261. Web. 2 May 2014. <<http://www.atmel.com/Images/doc8161.pdf>>.

So:

$$\begin{aligned}
 V_{in} &= \frac{2000 \pm 1\%}{V_{out}(2000 \pm 20 + 2000 \pm 20)} \\
 V_{in} &= \frac{2000 \pm 1\%}{V_{out} 4000 \pm 1\%} \quad (3) \\
 V_{in} &= \frac{1 \pm 1\%}{(2 \pm 1\%)V_{out}}
 \end{aligned}$$

The uncertainty of the raw readings from the ADC is ± 1 potential difference unit^[23]. By multiplying by $\frac{5}{1024}$, this uncertainty is converted to the uncertainty of V_{in} : $\pm 0.0049V$.

Thus, from (3), it is deduced that the uncertainty of potential difference across the battery is:

$$\begin{aligned}
 \Delta V_{out} &= (1\% + 1\% + \frac{0.0049}{V_{in}})V_{in} \\
 \Delta V_{out} &= \frac{V_{in}}{50} + 0.0049
 \end{aligned}$$

Current was calculated from the potential difference across the shunt, and Ohm's Law:

$$I = \frac{V_{in}}{R_{shunt}}, \text{ where } R_{shunt} = 0.4\Omega \pm 3\%.$$

As calculated before, $\Delta V_{in} = 0.0049V$. Thus, the uncertainty of current was:

$$\Delta_I = \left(\frac{0.0049}{V_{in}} + 3\% \right) I$$

²³ Digital instrument: smallest interval

8.2.1 Handling fluctuating electrical power

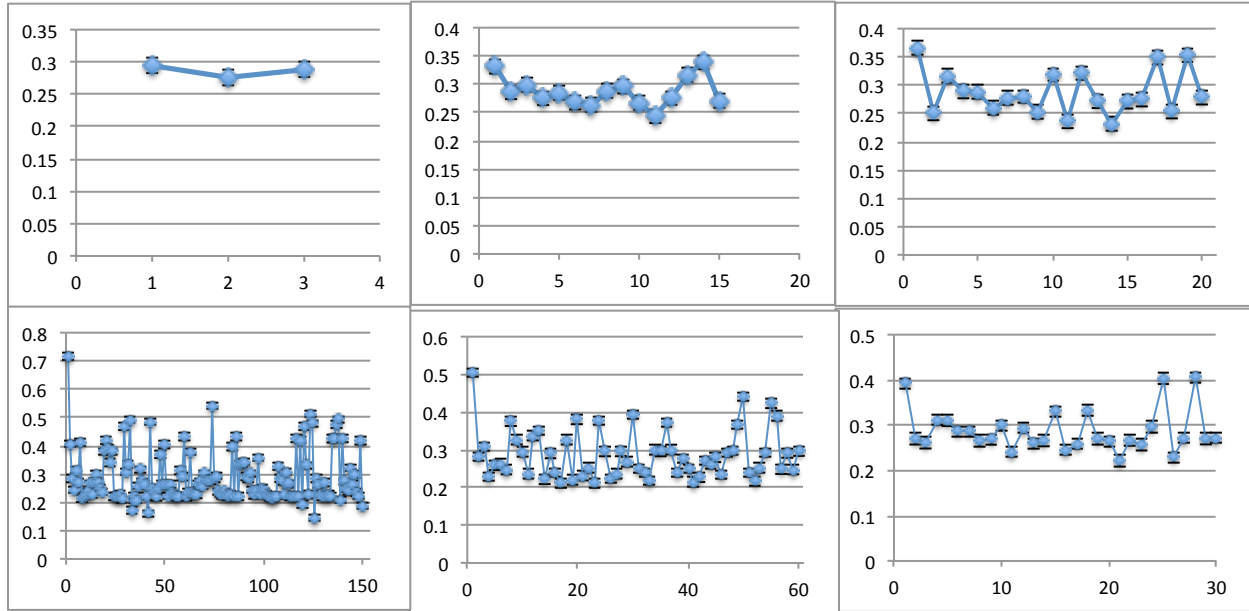


Fig 15. Mean current vs. time units of successively smaller sets of current data over 1500 samples for $1000\mu\text{s}$ -sampling-period 3-coil sequence. From top left, clockwise: 500 data points per mean, 100, 75, 50, 25, 10. Y-axis is current.

To deal with the constantly-changing current (Fig 14), the mean of the current and potential difference were taken over a large number of samples. Despite the fact that Fig. 15 shows the fluctuations in the mean of small sets of current samples over time, larger samples show that the current remains relatively constant throughout the test. As a result, in relevant calculations, it was assumed that the input power was constant, calculated using the mean of current and p.d. over many data points.

9.0: Calculations

9.1: Power

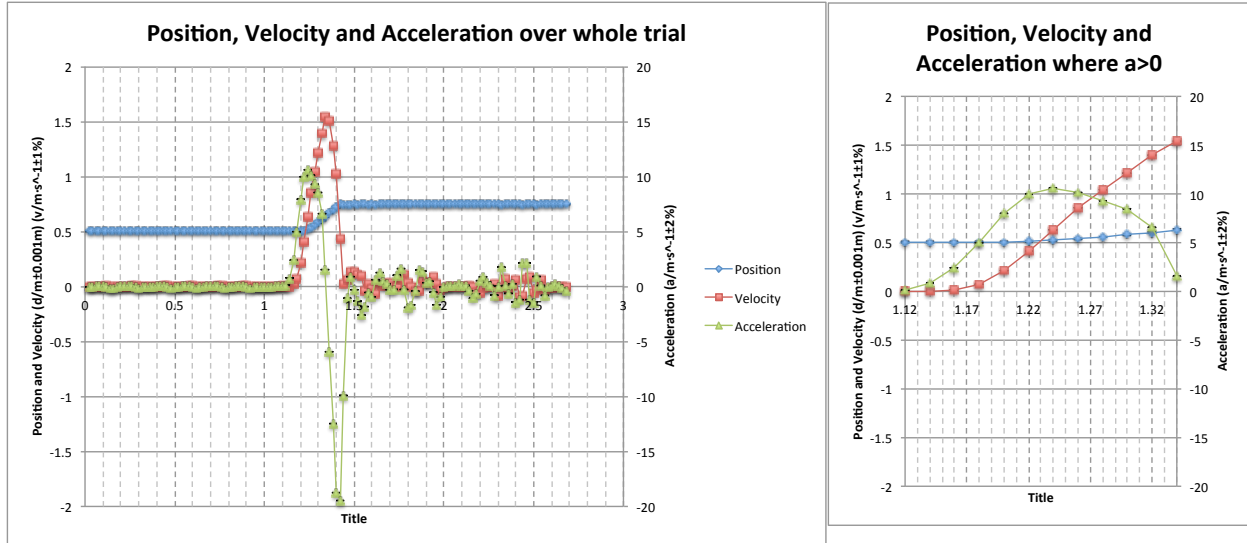


Fig 16 & 17. Graph showing the motion measurements taken over the entire trial (left) and isolation of the data during the motor's operation (right)

9.1.1: Output power

The range over which the motor's power efficiency was calculated and evaluated was identified by a computer program by the longest span of time during which the forcer had positive *acceleration* (Fig. 15 to 16) (*see Appendix 3 for source code*).

Power was determined over this time interval by the following relationship:

$$P = mv(t)a(t), \text{ where } v \text{ and } a \text{ are instantaneous.}$$

9.1.2: Input power

It was determined experimentally that the 3-coil "push" at the beginning of each trial drew ~470mA. A script was created to detect this current spike and take the arithmetic mean from that point to the point when the rod stopped moving forward. This time interval is the same as that of the output power (Fig 16 & 17) (*see Appendix 3 for source code*). The mean of the current was multiplied by the arithmetic mean of the potential difference over the same amount of time to find the input electrical power.

9.2: Efficiency over time

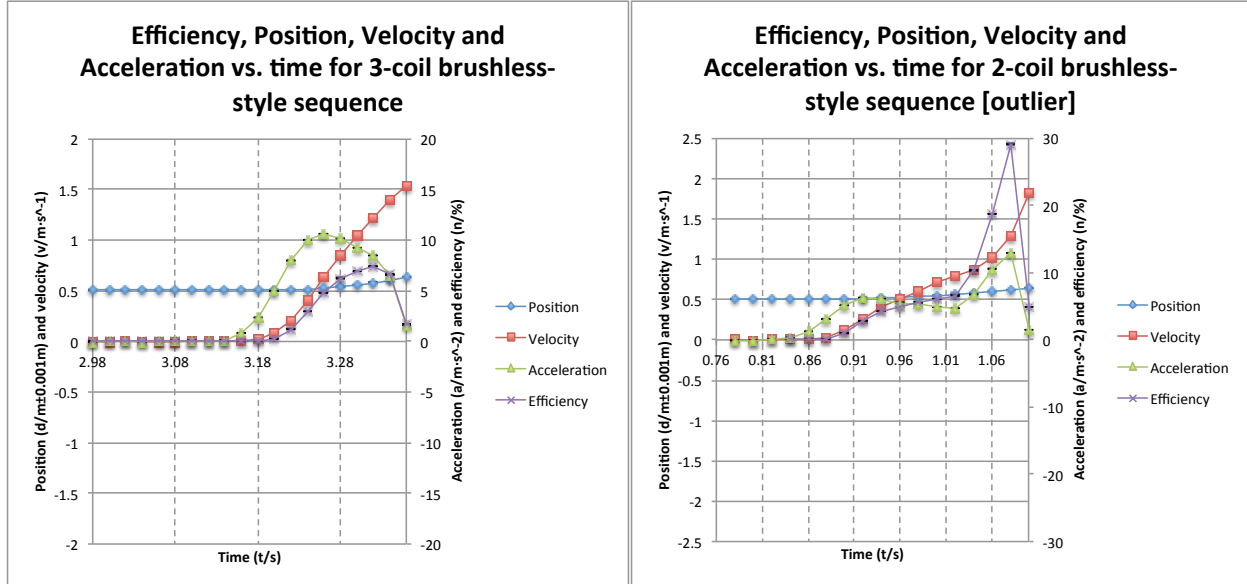


Fig 18 & 19. Sample graph of position (left y-axis), velocity (left y-axis), acceleration (right y-axis) and efficiency (right y-axis) for 3-coil operation (feedback sampling period = $1160 \pm 30 \mu\text{s}$) and an example of an outlier: notice the uncharacteristic spike in velocity at $t=1.10\text{s}$ (feedback sampling period: $760 \pm 30 \mu\text{s}$)

The quotient between the previously-calculated output mechanical power and this input electrical power yields the efficiency of the system. Efficiency can be expressed by the formula:

$$\eta = \frac{m \cdot v(t) \cdot a(t)}{VI} \quad (\text{see Appendix 4 for sample output})$$

The efficiency uncertainty is estimated from previous calculations' results (where ϵ_x is the percent uncertainty of the variable x):

$$\epsilon_\eta = \epsilon_m + \epsilon_v + \epsilon_a + \epsilon_V + \epsilon_I, \quad \epsilon_v \approx 0.5\%, \quad \epsilon_a \approx 0.5\%, \quad \epsilon_V = (2\% + \frac{0.0049}{V_{in[V]}}), \quad \epsilon_I = (\frac{0.0049}{V_{in[I]}} + 3\%), \quad \epsilon_m = \frac{0.001}{28.068}$$

$$\Delta_\eta \approx 0.003\% + 0.5\% + 0.5\% + (3\% + \frac{0.0049}{7.50}) + (3\% + \frac{0.0049}{0.20}) \quad \text{assuming } V_{\text{battery}} \approx 7.50\text{V}, I_{\text{tot}} \approx 0.20\text{A}$$

$$\Delta_\eta \approx 9\%$$

The relationship between efficiency, velocity and acceleration at constant input power can be seen in Fig. 18. Efficiency was calculated for each trial of each sampling time, as shown in Fig. 20. The discrepancies between each trial were usually not large, but sometimes there were significant outliers (e.g. Fig 19).

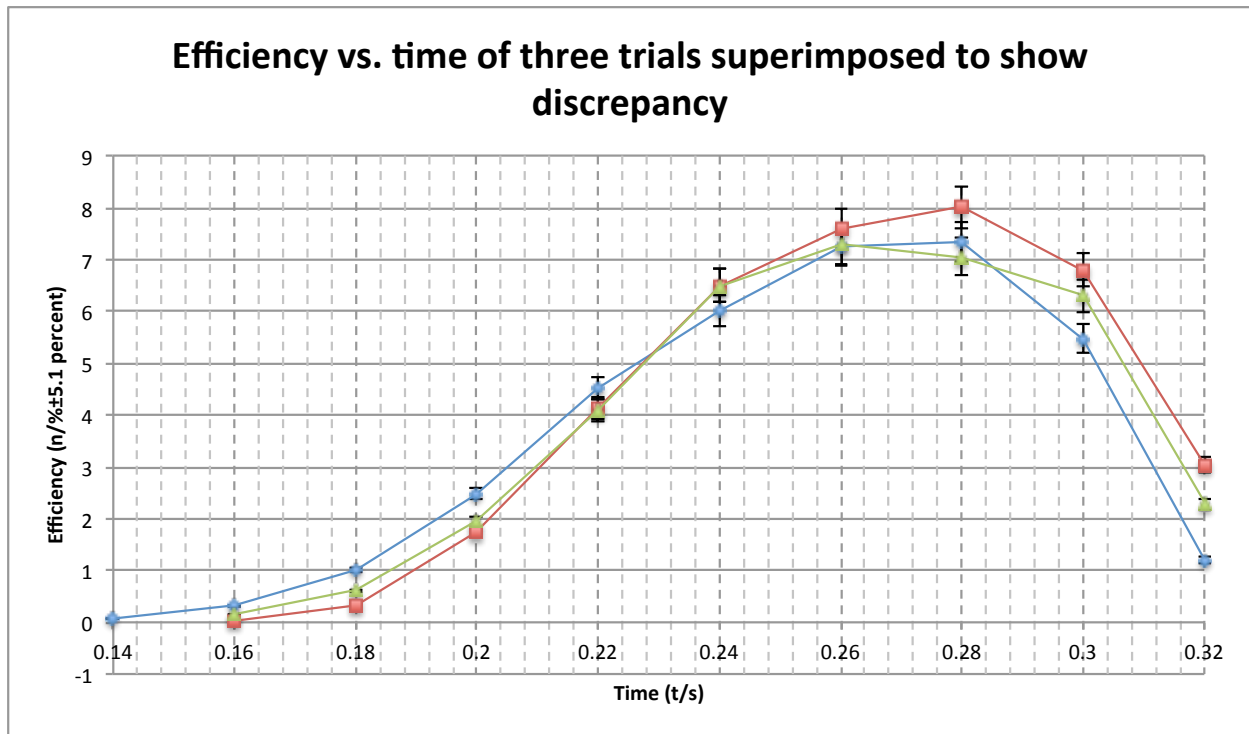


Fig 20. Sample graph showing discrepancies in efficiency vs. time between the three trials for the 1360 μ s-sampling-period, 3-coil sequence.

(See Appendix 4 for comparisons of efficiency-time graphs for each sampling period)

10.0: Comparisons and Conclusions

10.1: Comparison of maximum power efficiencies and energy efficiencies of each sequence

As mentioned in the introduction, two metrics derived from the efficiency calculations are used to compare the efficiency of the sequences.

The first is the maximum power efficiency attained by the motor. Given that the range of the motor was the same for all trials, the one that attained the highest efficiency in that range had the highest potential to be efficient when loads are applied. The arithmetic mean of the maximum efficiency attained by each trial for each feedback sampling period of each commutation sequence was calculated, and the sampling period with the maximum mean for each sequence was compared against each other. For simplicity's sake, the uncertainty is calculated as the sum of the largest of the differences between each maximum and the mean and twice the estimated percent uncertainty of efficiency: $\max(|\eta_{mean} - \eta_n|) + 2 \cdot (6\%)$.

Table 6 - Comparing mean maximum efficiency ($\eta/\%$) between sequences

| | | Commutation sequence | | |
|---|-----------|----------------------|---------------|-----------|
| | | 1-coil | 2-coil | 3-coil |
| Sampling period | 560±30µs | 3.7±0.6 | 4.6±1.6 | 15±6 |
| | 760±30µs | 4.5±0.6 | 15±16 | 13±3 |
| | 960±30µs | 4.7±1.1 | 8.8±3.9 | 6.9±1.7 |
| | 1160±30µs | 6.2±0.9 | 8.5±2.2 | 7.3±0.9 |
| | 1360±30µs | 6.1±1.3 | 9.4±1.6 | 7.5±1.4 |
| Maximum | | 6.2±0.9 | 15±16 | 15±6 |
| Maximum lowest possible value ($\max(\eta-\Delta\eta)$) | | 6.2±0.9 [5.3] | 9.4±1.6 [7.8] | 13±3 [10] |

The second is the energy efficiency over the range of the motor's operation. Simply put, it is the ratio of the useful, kinetic energy gained by the forcer and the energy supplied by the battery. It can also be represented by the ratio of the integrals of output power

and input power – $\eta = \frac{\int_{t_i}^{t_f} P_{out}(t) dt}{\int_{t_i}^{t_f} V(t)I(t) dt}$. This form is convenient if input electrical power

fluctuates significantly over time. However, since it is assumed that it doesn't, this can be simplified to:

$$\eta_E = \frac{m}{2} \frac{v_f^2 - v_i^2}{P_m \Delta t}.$$

As previously mentioned, this metric is used to determine which motor is most efficient at this range or shorter ranges. Like for maximum power efficiency, the arithmetic mean of the energy efficiency values for each sampling period were calculated, and the maximum mean was used to compare the sequences. The uncertainty is calculated as the largest of the differences between each efficiency result and the mean efficiency.

Table 7 - Comparing mean energy efficiency ($\eta/\%$) between sequences

| | | Commutation sequence | | |
|--|-----------|----------------------|---------------|---------------|
| | | 1-coil | 2-coil | 3-coil |
| Sampling period | 560±30µs | 2.3±0.5 | 2.8±0.9 | 5.9±2.3 |
| | 760±30µs | 2.4±0.7 | 6.4±6.4 | 7.3±0.9 |
| | 960±30µs | 2.8±1.1 | 4.8±2.6 | 3.3±1 |
| | 1160±30µs | 3.7±0.8 | 4.6±1.3 | 3.1±0.5 |
| | 1360±30µs | 3.4±0.7 | 4.6±1.4 | 3.9±1.8 |
| Maximum | | 3.7±0.8 | 6.4±6.4 | 7.3±0.9 |
| Maximum lowest possible value (max($\eta_E - \Delta\eta_E$)) | | 3.7±0.8 [2.9] | 4.6±1.3 [3.3] | 7.3±0.9 [6.4] |

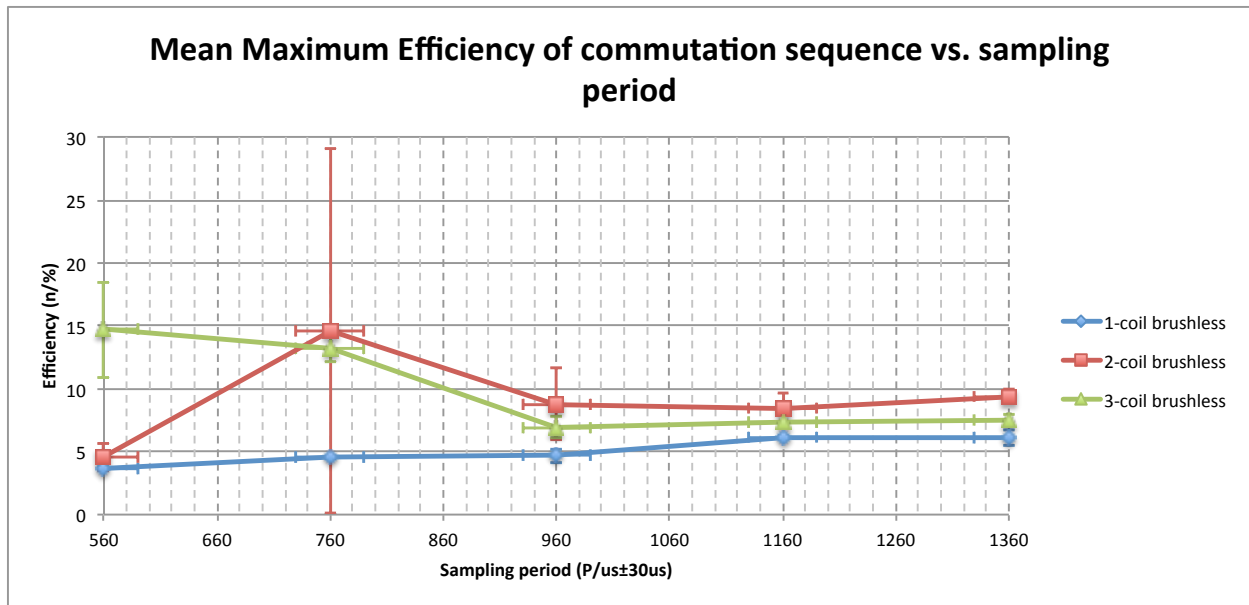


Fig 21. Graph showing mean maximum efficiency vs. sampling period for each commutation sequence

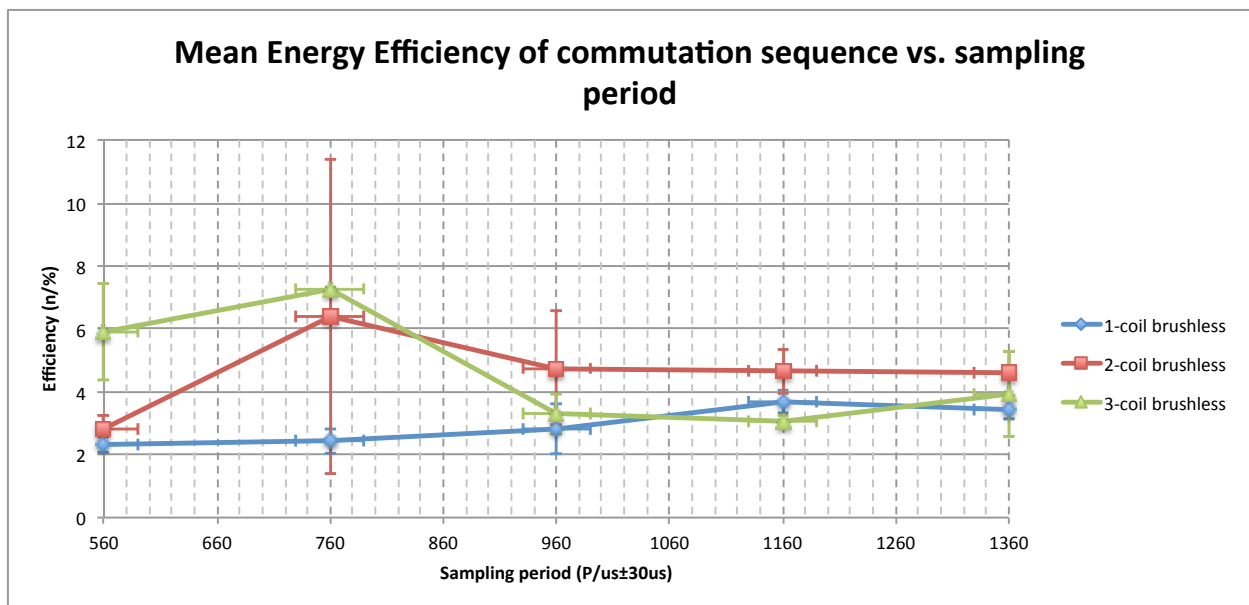


Fig 22. Graph showing mean energy efficiency vs. sampling period for each commutation sequence

10.2: Conclusion

Upon initial inspection, Table 5 seems to show that the 2-coil brushless sequence is the most efficient, operating at 14.62% efficiency at $P_{\text{sample}}=760\pm 30\mu\text{s}$. However, the magnitude of the uncertainty associated with this reading indicates that this high efficiency value was likely caused by an outlier (see Fig 12). By instead comparing the maximum value *after* subtracting the uncertainty, the trend that efficiency increases

with increased energized coils per phase becomes clear. The same goes for the energy efficiency, except the efficiency 3-coil sequence at $P_{\text{sample}}=760\pm 30\mu\text{s}$ is *even higher* than the 2-coil *outlier* at $P_{\text{sample}}=760\pm 30\mu\text{s}$. This trend can generally be explained by analyzing how the forces affect the efficiency of the motor.

Suppose a magnet is within the stator and is exactly one pitch distance from the next active coil. It is moving at an initial velocity $v_i \neq 0$. There are four forces acting on the magnet: the applied force from the magnetic field generated by the coils F_a , the resistive force of the mechanical load F_l , the resistive force of friction F_f and the resistive force from the induced current F_{md} . For the magnet to accelerate overall in travelling to the next coil, it must be true that:

$$\int_0^{t_f} F_a(t) dt > \int_0^{t_f} F_l(t) + F_f(t) + F_{md}(t) dt$$

where t_f is the time it takes for the magnet to travel to the next coil. This is because Newton's second law states:

$$\int_{t_i}^{t_f} F(t) dt = m \int_{t_i}^{t_f} a(t) dt = m(v(t_f) - v(t_i)) = \Delta p ;$$

for acceleration to occur to an object with constant mass, there must be a net change in momentum.

It is known that the induced force is directly proportional to the induced current^[24], and that the induced current is proportional to speed (*see Appendix 2 for proof*). The force of dynamic friction depends solely on the normal force, so if the motor does not change orientations or mass, the force of friction does not change. In the experiment, there was no load, so $F_l = 0$. The larger the proportion of the applied force to friction, the more efficient the phase, since a larger fraction of the electrical energy is going into doing mechanical work rather than overcoming friction. As a result, intuitively, more coils energized per phase should be better.

²⁴ Robertson, Will, Ben Cazzolato, and Anthony Zander. "Axial Force between a Thick Coil and a Cylindrical Permanent Magnet: Optimising the Geometry of an Electromagnetic Actuator." IEEE 48.9 (2012): 3. IEEE. Web. 4 May 2014. <<http://personal.mecheng.adelaide.edu.au/will.robertson/research/2012-magcoil.pdf>>.

However, because the acceleration is higher, F_{ind} increases faster as well, leading to a decrease in the net force in the desired direction. If this happens too quickly, the ratio of this net force and friction decreases, potentially counteracting the higher F_a .

To where it decreases and when depends on the range of the motor, and the results shows that the range of a linear motor is too short for this to occur. Instead, the former phenomenon appears to be dominant in this system, meaning for short distances it is more efficient to energize more coils per phase than the converse.

However, this does not completely explain the trend of efficiency within each sequence vs. sampling period. While the efficiency for the 1- and 2-coil sequences are positively correlated with sampling period, the 3-coil sequence is significantly more efficient at higher sampling rates, suggesting that it might suffer greatly from a decrease in sampling rate, while other sequences gain from the increased applied force vs. friction force ratio.

11.0: Possible improvements

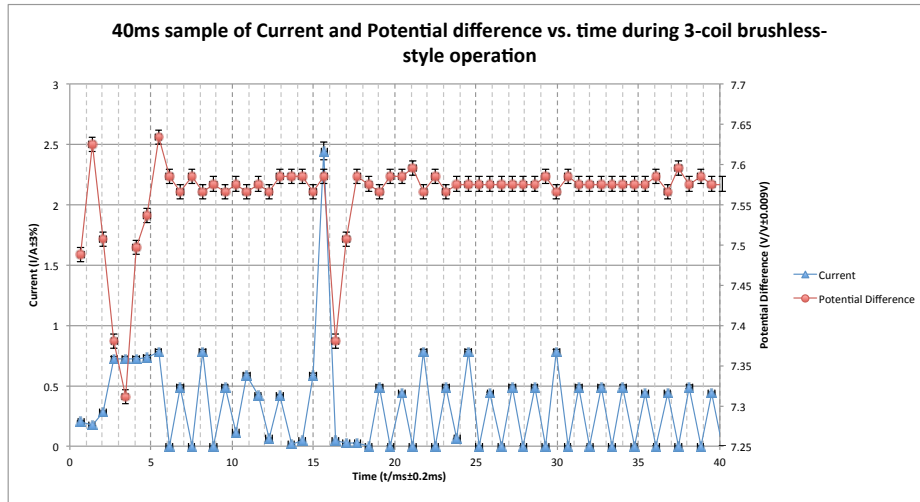


Fig 23. Fig. 14 repeated for clarity.

Both the Go!Motion sensor and ammeter proved to be the largest sources of error due to a lack of bandwidth. Because each trial ended abruptly, the former's maximum 50Hz sampling rate left a 20ms window at the end of tests during which the speed of a forcer accelerating at $10\text{m}\cdot\text{s}^{-2}$ (which is not unrealistic at the end of a test) would vary by up to $0.2\text{m}\cdot\text{s}^{-1}$, or 10-20% of the recorded speed for most trials. For the latter, the problem is one of curve folding. From Fig. 22 it appears as though, from $t=20\text{ms}$ onward, the duty cycle of the current is 50%. However, for 3-coil operation at $P_{\text{sample}}=1160\mu\text{s}$, the duty cycle is $\sim \frac{1000}{1160} \approx 86\%$. The discrepancy is caused by the fact that the sampling rate was

near the Nyquist frequency of the : twice the frequency of the feedback sampling ($f_{\text{sample}}\cdot 2=1720\text{Hz}$) and the minimum frequency needed to resolve the shape of the wave. At this frequency it is likely that the values read are not accurate due to a misrepresentation of the duty cycle of the curve. These can add up to a massive difference in the final efficiency calculation. Both limitations should be rectified by an increase in bandwidth.

12.0: Bibliography

"8-bit AVR® Microcontroller with 4/8/16/32K Bytes In-System Programmable Flash." ATMEL (n.d.): Web. 2 May 2014. <<http://www.atmel.com/Images/doc8161.pdf>>.

Cupertino, Francesco, Paolo Giangrande, Gianmario Pellegrino, and Luigi Salvatore. "End Effects in Linear Tubular Motors and Compensated Position Sensorless Control Based on Pulsating Voltage Injection." IEEE58.2 (2011): IEEE. Web. 30 Apr. 2014.

Halliday, David, and Robert Resnick. Fundamentals of Physics. II ed. Vol. I. United States: John Wiley & Sons, 1981. Print. Extended Version.

"How Does Logger Pro Calculate Velocity and Acceleration from Motion Detector Data?" Vernier Tech Info Library. Venier, 11 Jan. 2011. Web. 11 May 2014. <<http://www.vernier.com/til/1011/>>.

Hygenic Servotube Actuator. Dunker Motoren Linear Systems, n.d. Web. 11 Apr. 2014. <http://www.dunkermotoren.com/data/linearsysteme/downloads/DS01102_EN.pdf>.

Kim, Won J., M. T. Berhan, D. L. Trumper, and J. H. Lang. "Analysis and Implementation of a Tubular Linear Motor with Halbach Magnet Array." Analysis and Implementation of a Tubular Motor with Halbach Magnet Array (1996). IEEE. Web. 29 Apr. 2014. <http://ieeexplore.ieee.org/xpl/login.jsp?tp=&arnumber=557069&url=http%3A%2F%2Fieeexplore.ieee.org%2Fxppls%2Fabs_all.jsp%3Farnumber%3D557069>.

Murphy, Bryan C., and Won J. Kim. "Development of a Novel Direct-Drive Tubular Linear Brushless Permanent Magnet Motor" Internationalal Journal of Control, Automation and Systems 2.3 (2004). IJCAS. Web. 2 Apr. 2014. <http://www.ijcas.org/admin/paper/files/IJCAS_v2_n3_pp279-288.pdf>.

Robertson, Will, Ben Cazzolato, and Anthony Zander. "Axial Force between a Thick Coil and a Cylindrical Permanent Magnet: Optimising the Geometry of an Electromagnetic Actuator." IEEE 48.9 (2012). IEEE. Web. 4 May 2014. <<http://personal.mecheng.adelaide.edu.au/will.robertson/research/2012-magcoil.pdf>>.

Silva, C., Asher, G.M. and Sumner, M., "Hybrid rotor position observer for wide speed ranger Sensorless PM motor drives including zero speed", IEEE Transactions on Industry Electronics, Vol. 53, N° 2, April 2006.

APPENDIX I - Signages of Vectors and associated Scalar Quantities

The following definitions are clarified here to avoid ambiguity of the directional terms forward, backwards, clockwise and anticlockwise; and of the signages positive and negative.

A1.1 Coils

The vector area of a coil's surface \vec{A} is represented by an arrow orthogonal to the coil's surface plane whose magnitude is equal to the scalar magnitude of the coil's area. The positive direction, also herein known as the "forward direction" of the unit vector herein represented as \hat{A} defines the "positive" direction of curl around the current loop. An observer looking at the coil in the positive \hat{A} direction will remark that positive charges flowing clockwise around the coil will produce a magnetic field in the positive \hat{A} direction along the axis of symmetry. Current in this direction will herein be referred to as "positive" current. Conversely, the magnitude of a potential difference across a broken loop of wire that becomes progressively more *negative* in the clockwise direction is positive.

A1.2 Magnets

Let \hat{M} be the unit vector that lies on a magnet's axial axis of symmetry and points from the magnet's south pole to a magnet's north pole. All displacements are relative to the magnet's north pole in this direction unless otherwise specified.

A1.3 Forcer

Displacements and velocities regarding the forcer will be relative to its direction of motion during each trial. All references are made while the forcer is in motion, so there is no need to define orientation for the static forcer.

APPENDIX 2 - Elaboration on Theory behind Sensorless Operation

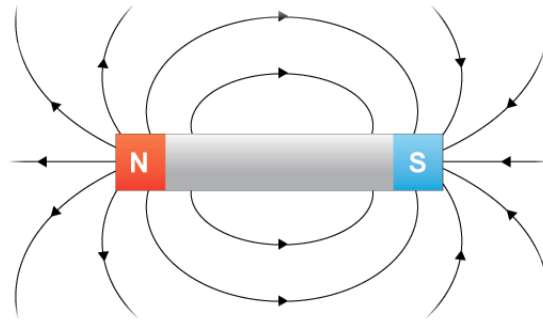


Figure 24: simplified diagram of magnetic field \mathbf{H} around dipolar magnet

While the magnetic field of a permanent magnet appears to arise from “thin air”, in reality, it is the product of currents on the atomic scale caused by the combination of asymmetries in the atoms’ electron configurations and the intrinsic magnetic moments of elementary particles. As a result, this magnetic field can be closely represented by different configurations of infinitely-thin current-carrying wire. The magnetic field of a cylindrical magnet – a shape of particular significance to this experiment – closely resembles the magnetic field from a planar, infinitely thin current loop at large distances (i.e. $z \gg 1$). Approach this coil, however, and this model becomes progressively less accurate due to the magnet’s length in the \hat{z} direction. Instead, it is necessary to extend the current loop in the \hat{z} direction and create a *sheet* of current comprised of an infinite number of infinitely thin, concentric current loops carrying infinitesimal amounts of current. Instead of representing current as the time rate of change passing through a single point in space, we can use the time rate of charge passing through a *line*. This metric is known as surface current density J , measured in $\text{A}\cdot\text{m}^{-1}$. It becomes invaluable for calculating the surrounding magnetic field of current sheets, as the finite current arguments I for some magnetic field equations can be replaced by $J \cdot dz$: the current density over an infinitesimal strip which degenerates into a current loop. The Biot-Savart law is one such equation that takes the cylindrical coordinates of a point $P(r,\vartheta,z)$ in proximity to a current loop whose magnitude of current is constant at all points along its surface, and returns the radial and axial components of the magnetic field strength at that point. It takes the form of the following equations^{[25][26]}:

²⁵ Yee, M. (2009). Magnetic Trapping and Transport of Ultracold Atoms. Retrieved June 20, 2014, from <http://ultracold.physics.utoronto.ca/reprints/YeeB>

²⁶ **Note:** in ²³, there appears to be an error in equation (3.6): $B_z(0,0)$ in (3.6) $\neq B_z(0)$ in (3.3), *unless* (3.6) is divided by z .

$$B_r(r, z, I) = \frac{\mu_0 I}{2\pi r} \cdot \frac{z}{[(R+r)^2 + z^2]^{1/2}} \left[-K(k^2) + \frac{R^2 + r^2 + z^2}{(R-r)^2 + z^2} \cdot E(k^2) \right] \quad (4)$$

$$B_z(r, z, I) = \frac{\mu_0 I}{2\pi} \cdot \frac{1}{[(R+r)^2 + z^2]^{1/2}} \left[K(k^2) + \frac{R^2 - r^2 - z^2}{(R-r)^2 + z^2} \cdot E(k^2) \right] \quad (5)$$

$$k^2 = \frac{4Rr}{(R+r)^2 + z^2}$$

$$K(k^2) = \int_0^{\frac{\pi}{2}} \frac{1}{\sqrt{1 - k^2 \sin^2 x}} dx$$

$$E(k^2) = \int_0^{\frac{\pi}{2}} \sqrt{1 - k^2 \sin^2 x} dx$$

where $K(k^2)$ is the elliptical integral of the first kind, $E(k^2)$ is the elliptical integral of the second kind^[27], I is the current flowing through the current loop, R is the radius of the current loop and the pair (r, z) are components of the cylindrical coordinate definition of P (the field is cylindrically symmetric for the cylindrical magnets, so ϑ does not matter). While R and r must be ≥ 0 , z and I can be either positive or negative, and are related to each other by the right-hand rule as described in *Appendix 1*. A positive z value implies that P is on the “north” end of the current loop, and vice versa.

Substituting I for $J \cdot dz$, equations (4) and (5) become:

$$dB_r(r, z, J) = \frac{\mu_0 J}{2\pi r} \cdot \frac{z}{[(R+r)^2 + z^2]^{1/2}} \left[-K(k^2) + \frac{R^2 + r^2 + z^2}{(R-r)^2 + z^2} \cdot E(k^2) \right] dz \quad (6)$$

$$dB_z(r, z, J) = \frac{\mu_0 J}{2\pi} \cdot \frac{1}{[(R+r)^2 + z^2]^{1/2}} \left[K(k^2) + \frac{R^2 - r^2 - z^2}{(R-r)^2 + z^2} \cdot E(k^2) \right] dz \quad (7)$$

where J is constant and yet to be determined.

The integral from the north pole to the south pole — or z and $z+l$ respectively, where z is the z -axis displacement of the north pole and l is the length of the magnet — yields the overall magnetic field strength at P :

²⁷ Ibid.

$$B_r(r, z, J) = \int_z^{z+l} dB_r(r, z, J)$$

$$B_z(r, z, J) = \int_z^{z+l} dB_z(r, z, J)$$

We will define an arbitrary function that will be useful in determining the back EMF from a moving permanent magnet later:

$$G_z(r, z) = \frac{1}{J} \frac{dB_z(r, z, J)}{dz} \quad (10)$$

Force on current loop:

The force acting on a current loop is equal to the product of the magnitude of the current and the surface integral of the cross product of the magnetic field strength and the infinitesimal length element:

$$\vec{F} = |\vec{I}| \oint \vec{B} \times d\vec{l} \quad (10)$$

Imagine a cylindrical current sheet concentric to a current loop: a single subunit of our linear motor. We will examine the force on the current loop caused by the magnetic field of the current sheet. Due to the magnetic field's cylindrical symmetry and the concentricity of the current loop and the current sheet, (10) can be simplified to:

$$F(R, z) = |\vec{I}| \cdot 2\pi R \cdot B_r(R, z, J) \quad (11)$$

where R is the radius of the current loop. To explain: the result of $\vec{B}_z(r, z, J) \times d\vec{l}$ is in the radial direction and $|\vec{B}_z(r, z, J)|$ is constant for constant $|r|$ and constant z , thus

$\oint_C \vec{B}_z(r, z, J) \times d\vec{l} = 0 \cdot \hat{r}$ over any planar, concentric circular path C. On the other hand,

$\vec{B}_r(r, z, J) \times d\vec{l}$ is in the axial direction and $|\vec{B}_r(r, z, J)|$ is also constant for constant $|r|$ and constant z , thus $\oint_C \vec{B}_r(r, z, J) \times d\vec{l} = 2\pi R \cdot \vec{B}_r(R, z, J)$ over any planar, concentric circular path C

with radius R (equivalent to finding the area of the curved face of a cylinder with height $B_r(R,z,J)$).

The loops in the coil are assumed to be sufficiently tightly packed such they cannot move independently. Thus, the force on the coil as a whole is assumed to be the sum of the force on each individual loop.

Based on the geometry of the stator scaffold, the thickness of the wire and the dimensions of each coil, it was estimated that each coil consisted of five levels of 55 closely-packed loops, resulting in 275 loops in total. It was assumed that the wires were sufficiently thin and the loops were sufficiently planar that the spiral nature of the coil could be ignored and the loops could be modelled as the infinitely-thin planar loops used in the theoretical model.

Under this assumption, each loop is separated by $\frac{5.9 \pm 0.1mm}{55} = 1.1 \times 10^{-1} \pm 0.2 \times 10^{-1}mm$

axially and $1.01 \times 10^{-1}mm$ radially²⁸. Let:

$$S(f) = \sum_{k=0}^5 \sum_{n=0}^{55} f(w + sk, \frac{5.9 \times 10^{-3}}{55}n) \quad (14)$$

$$w = 4.9295 \times 10^{-3}m$$

$$s = 1.01 \times 10^{-4}m$$

Then:

$$F_{tot} = S(F) \quad (15)$$

$|\bar{I}|$ is set to an arbitrary, positive, non-zero, real number for the purposes of this illustration.

Potential difference across current loop:

By definition, the magnetic flux through a surface S is equal to the integral of the dot product of the magnetic fields strength and the infinitesimal unit area, or the volume under the x, y, \bar{B}_z graph:

²⁸ http://en.wikipedia.org/wiki/American_wire_gauge

$$\Phi = \oint_S \vec{B} \cdot d\vec{A} = \oint_S B_z(r, z, J) \cdot dA$$

The second equality is true in our particular situation because there is no component of the radial magnetic field in the direction \hat{A} .

Thanks to the circular shape of the coil and the cylindrical symmetry, this can be solved as a much simpler volume of rotation problem, where the B_z, r graph is rotated about the z axis. Using the cylinder method, we arrive at the equation:

$$\Phi(z) = 2\pi \int_0^R r \cdot B_z(r, z, J) dr \quad (12)$$

Lenz's law states that the potential difference across a coil is equal to *negative* the time rate of flux through the coil, or:

$$\varepsilon = -\frac{d\Phi}{dt} \quad (13)$$

Using (12) and (13), the potential difference across a current loop bound by S is the following:

$$\varepsilon = -\frac{d(2\pi \int_0^R r \cdot B_z(r, z, J) dr)}{dt} = -\frac{dz}{dt} \frac{d(2\pi \int_0^R r \cdot B_z(r, z, J) dr)}{dz} = -v_z \frac{d(2\pi \int_0^R r \cdot B_z(r, z, J) dr)}{dz} \quad (13)$$

Putting the differential of the equation in terms of dz instead of dt gives us the chance to make a massive simplification.

Recall $G_z(r, z, J) = \frac{1}{J} \frac{dB_z(r, z, J)}{dz}$. Substituting into (13):

$$\varepsilon = -J \frac{d(2\pi \int_0^R r \cdot \int_z^{z+l} G(r, z) dz dr)}{dz} = -J \frac{d(2\pi \int_0^R \int_z^{z+l} r \cdot G(r, z) dz dr)}{dz}, \text{ since } r \text{ is treated as a constant in the second integral, which is in terms of } dz.$$

Because the points $[(R,z+1),(R,z),(0,z+1),(0,z)]$ form a rectangle on the (r,z) graph, no manipulations need to be made to the domain of either integral for them to be reversed, thus:

$$\varepsilon(R,z) = -2\pi Jv \frac{d\left(\int_0^{z+l} \int_0^R r \cdot G(r,z) dr dz\right)}{dz} = -2\pi Jv \left(\left(\int_0^R r \cdot G(r,z) dr\right) \circ (z+l) - \left(\int_0^R r \cdot G(r,z) dr\right) \circ (z)\right)$$

Since $G(r,z)$ has no correlation to the value of v (neither within the function nor the integral since no component of G is correlated with acceleration), the equation above also shows an interesting property of back EMF: that it is *directly proportional* to negative velocity.

Unfortunately, $G(r,z)$ is not solvable analytically. The best we can do is compute a precise estimate. Luckily, with modern computers, this estimate is quite accurate indeed.

By Kirschoff's Voltage Law, the potential difference across a coil consisting of many loops connected in series is equal to the sum of the potential difference across each individual loop. Using (13), the potential difference across the coil as a whole is equal to:

$$\varepsilon_{tot} = JvS(\varepsilon) \quad (16)$$

J was calculated by solving $H(0,0,J) = 0.4878T$: the value of the surface field strength provided by the manufacturers^[29]. This value turns out to be $4.016 \times 10^7 A \cdot m^{-1}$ for the magnets used in the experiment, though for the purposes of determining the shape of the $\varepsilon - z$ this value doesn't affect the result so long as it is non-zero. v is an arbitrary, positive, non-zero, real number.

Plotting force and potential difference vs. z

Using the incredibly powerful SciPy library and its built-in quad function, (15) and (16) were evaluated for incremental values of z differing by $1.01 \times 10^{-4} m$ from $-0.07373m$ to $0.101m$ for a total of 173 data points. The script can be found in [Appendix 3](#). The errors from the calculation were in the 10^{-6} order of magnitude or smaller according to the

²⁹ <http://www.magcraft.com/NSN0617>

SciPy output, and were ignored. Values for l and R were derived from the manufacturer's page and the SketchUp model (Fig. 25) respectively:

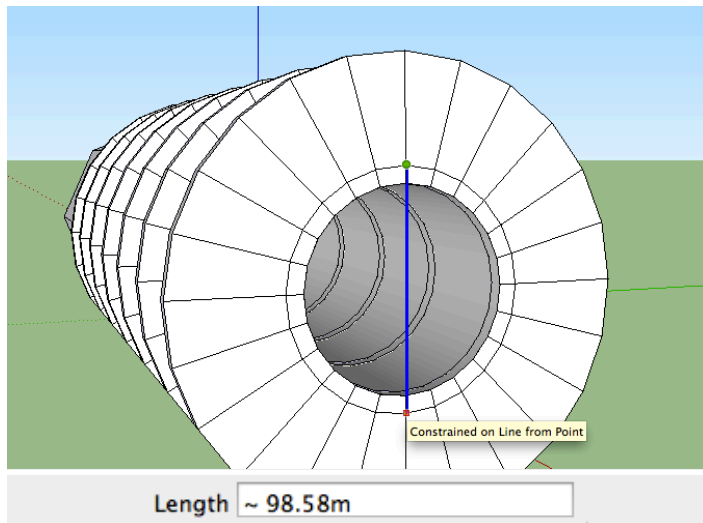


Figure 25: Measuring the diameter of the innermost coil layer. The model is scaled 10000:1 to obtain a more precise value. The measurement of 9.858mm is, for the sake of the illustration, taken to be an accepted value.

The calculated values were brought into Excel and graphed:

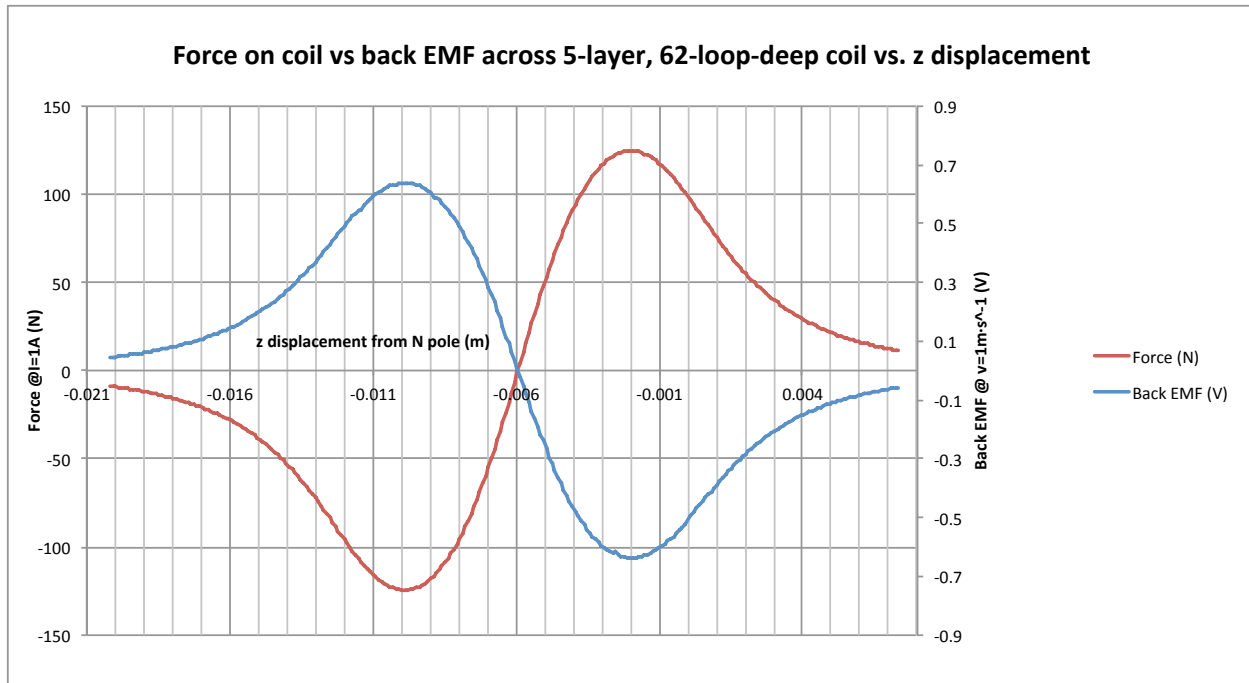


Figure 26: Back EMF and force vs. position for motor in operation

This graph shows that the force and the potential difference across the coil both reach extrema at the same displacements and, furthermore, that the graphs appear identical in shape. Consequently, energizing coils with the highest

magnitude of back EMF should therefore yield the highest magnitude of attractive or repulsive force. In this specific case, they are mirror images of each other on the x-axis, meaning that sending current in the positive direction when the back EMF is negative will yield to an applied force in the positive direction, and since v is positive, this will lead to positive acceleration. The opposite is also true. If, however, v is negative, both values would be the same sign in the same domains. In this case, sending current in the positive direction when the back EMF is negative will yield to an applied force in the *negative direction*, causing the coils to accelerate in the direction of its travel. The opposite is also true.

It is upon this principle that the sensorless motor operates. By sending current through the coil in the direction of *increasing* back EMF (i.e. “applying” a potential difference of opposite polarity than the back EMF across the coil), the \hat{A} component of the force must be in the direction of the \hat{A} component of the velocity. In this way, the forcer can be greatly accelerated with little computational effort.

As mentioned in 5.0 Independent Variable: Commutation Sequences, both the one- and two-coil sequences find the coil[s] with the highest absolute value of back EMF and energizes them. Aside from this convenient correlation in signage, the alignment of force and potential difference extrema in Figure 26 shows why this is optimal. In essence, the current-force ratio is maximized by energizing these coils.

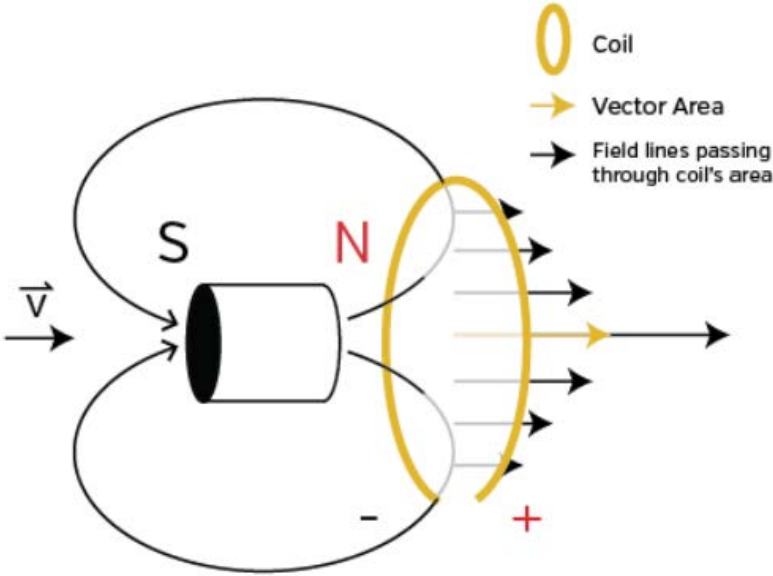


Figure 25: simplified diagram of magnet moving north-end first towards an open loop of wire. The p.d. across the wire is shown by the + and -.

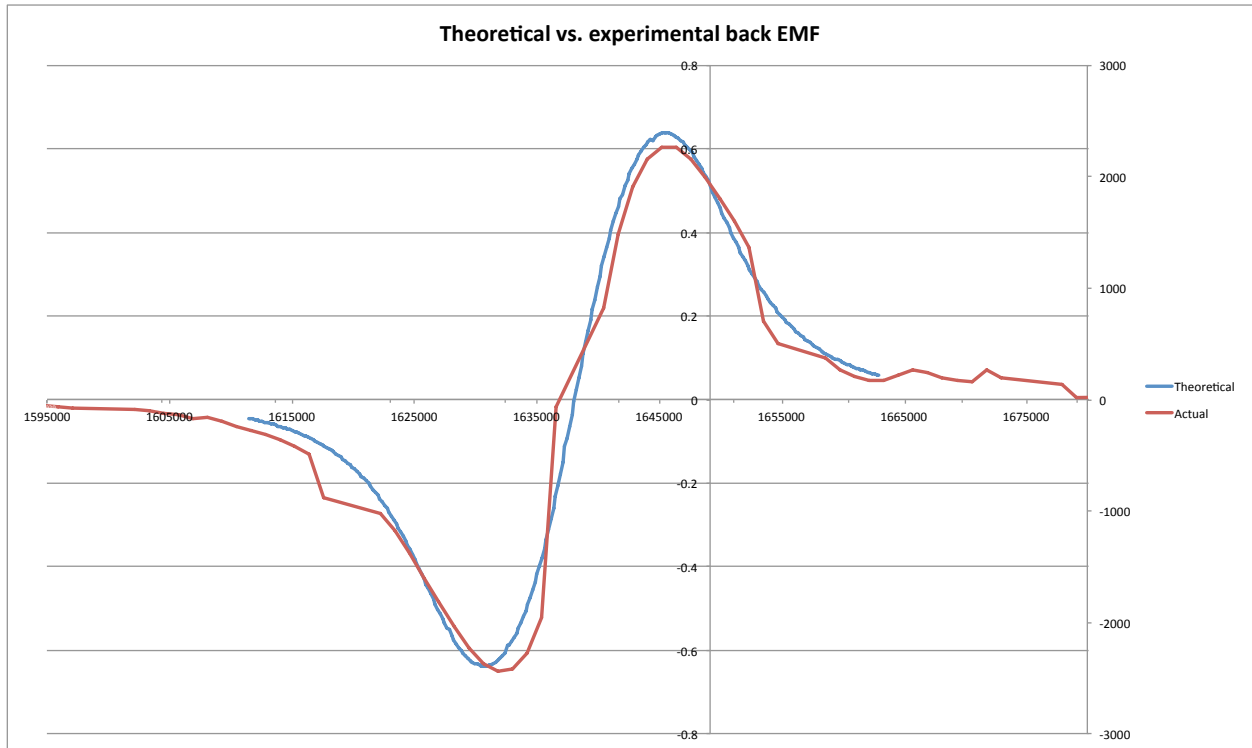
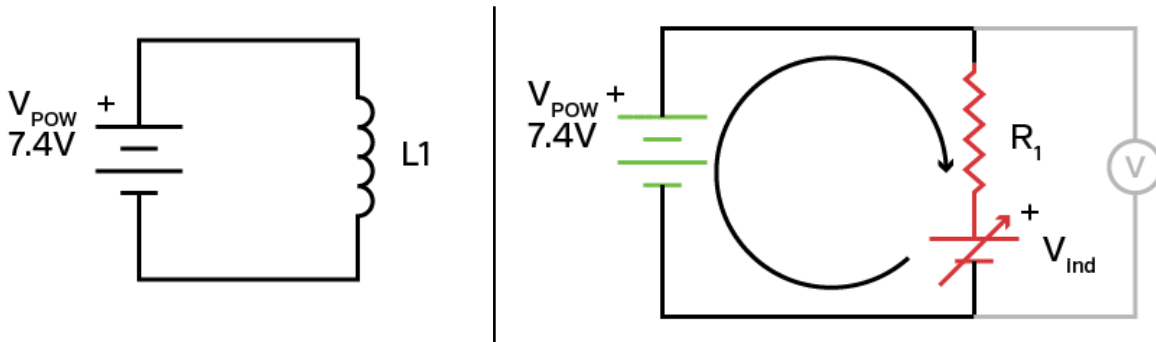


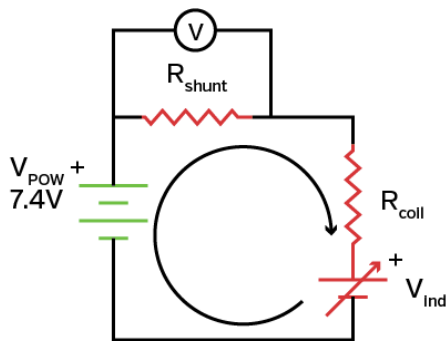
Figure 26: Theoretical potential difference across coil (blue, units in V, $v=1.0\text{m}\cdot\text{s}^{-1}$) vs. potential difference reading from test (red, units in $1/4096\text{V}$, v const.)

A note on operation: the reason that the coils are disengaged during measurement is because the potential difference across the coils when they are energized is equal to the potential difference across the battery, meaning the induced potential difference can't be measured directly this way. When a magnet's movement creates a potential difference on both ends of a coil, the coil can be represented by the equivalent circuit of an EMF source in series with a resistor.



Figures 27 & 28: Simplified schematic of an energized coil; equivalent circuit of coil with magnet moving near it and a voltmeter attached in parallel to coil (circular arrow denotes reference direction for potential difference in loop, green components are EMF sources while red components are EMF sinks)

The magnitude of the induced EMF is equal to the potential difference of the cell in the equivalent circuit. When the coil is energized, this circuit is connected in series to the power source, forming a closed loop. Kirchoff's second law states that the directed sum of the electrical potential differences around a closed loop must be equal to zero. Let the directed potential difference of the power source be positive. Because the current of the induced EMF in the coil flows opposite to the power source, the directed potential difference of this EMF must be negative. The absolute value of the sum of the potential difference across the resistor and the induced EMF is equal to the potential difference across the power source, meaning the induced potential difference and the power supply's potential difference are indistinguishable.



Alternatively, the potential difference across a shunt resistor placed in series to the coil is equal to $R_{shunt} I$, where I is the current through the circuit. This was used in the experiment to determine current through the circuit, but it has an alternative use: the relation can also be represented as $R_{shunt} \frac{(V_{pow} - V_{ind})}{(R_{shunt} + R_{coil})}$. If the

resistance of the coil when the coil is far from moving magnetic fields, and the potential difference across the power source are known, the induced potential difference can be determined easily.

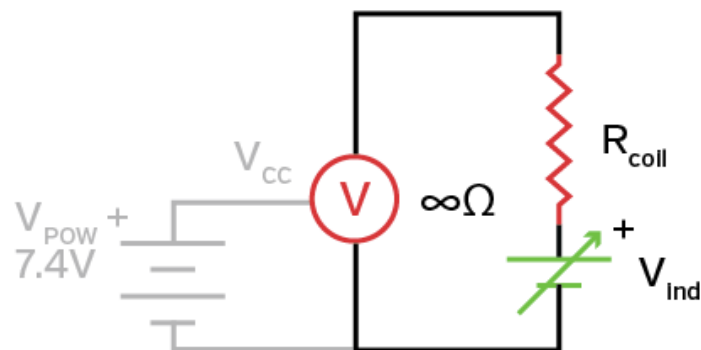
APPENDIX 2 - ELECTRONICS

THEORY OF OPERATION – ELECTRONIC DRIVE

Because the alternating polarity arrangement requires the capacity to drive a coil both ways, standard electrical switches like standalone transistors could not be used in the design, since they only allow current to flow one way during saturation; virtually no current flows otherwise. Instead, each pair of coils was connected to a half-H bridge (L298, 2A continuous per full H), which allows the current to flow in either direction. Each full H-bridge has four inputs, but when driving a pair of coils, the input to the upper and lower driver are always opposite, so only one microcontroller pin is needed; the other side is driven by an inverter. For normal high/low-side drivers, this is not always true as to stop current flow into the coil, both must be at the same potential. However, the L298 H-bridge comes with enable functionality for each half bridge, allowing the output to go into high-impedance mode.

THEORY OF OPERATION – ELECTRONIC ANALYSIS

Although the number of pins used per pair is the same (2) as using high/low-side drivers, having the high-impedance mode controlled directly by the state of a pin rather than the combination of the states of two pins is important for measuring feedback. For the ADC to measure feedback, the coil, which acts as an EMF source, must be connected to the same ground as the ADC like so:



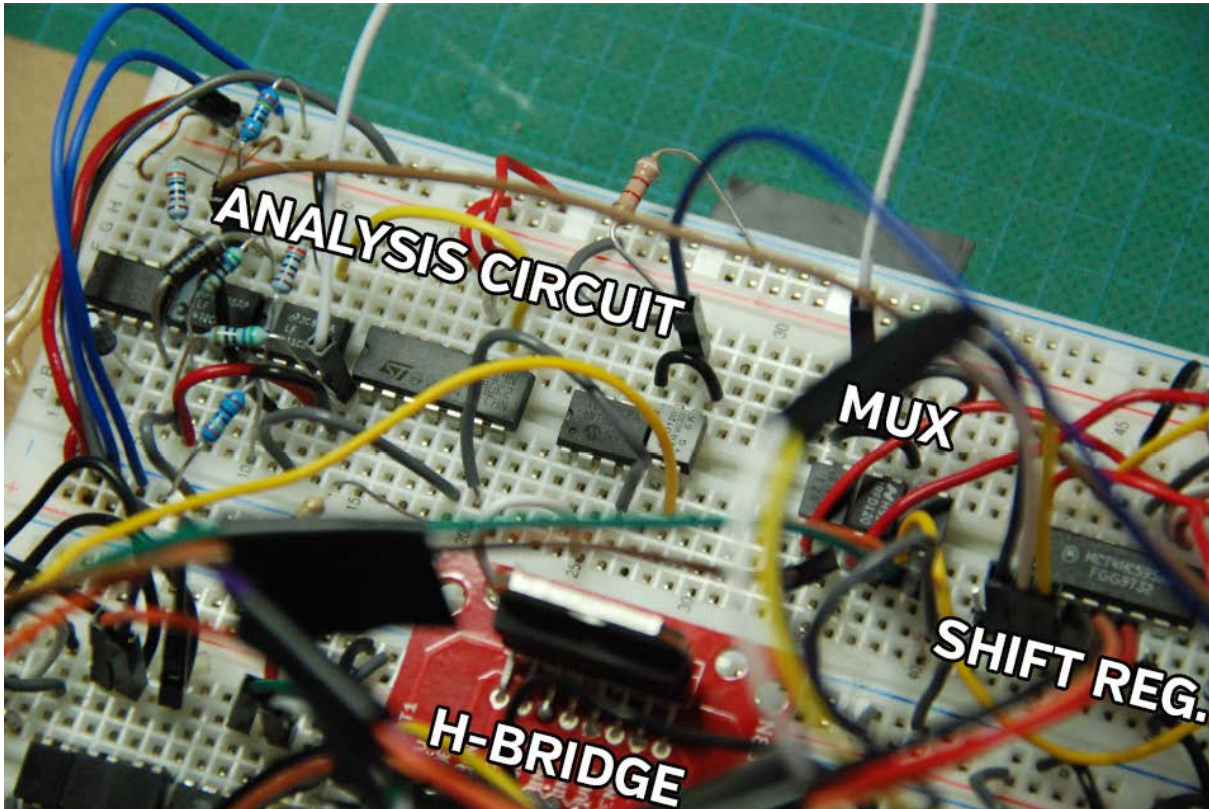
As a result, when measuring the feedback, all of the coils must be connected to ground. Using a transistor to control the connection to ground is easy with the inverted state of the enable pin.

One coil of each pair is connected to the source of three MOSFETs, which share a common drain, which is connected to the amplifier circuit. Each of these MOSFETs are individually controlled, so the feedback can be multiplexed, saving the space and cost of

using more pins and building more amplifier circuits, though at the expense of the artificial introduction of a sampling rate.

The ADC cannot handle the negative voltages that can arise from feedback, so all voltages must be converted to positive in order to be read. This “absolute value” functionality is achieved using the full-wave rectifier^[30].

Each pair of coils is connected to the drain of a MOSFET whose gate is connected to the respective half H-bridge enable. The MOSFET sinks the current when the bridge is disabled to create the same reference potential for the induced voltage as the potential the analogue-digital converter is referencing. The other end of the coil is connected to a multiplexer and is amplified for analysis by an operational amplifier circuit.



Figures 8: The analysis circuit (top-left, dense resistors, DIP-8 chips and diodes), multiplexer (center-right; three DIP-4 packages), shift register (far right) and H-bridge (bottom, red board)

³⁰ "Absolute Value Circuit (Full-Wave Rectifier)." Solutions -. Linear, June 2011. Web. 13 May 2014. <<http://www.linear.com/solutions/1608>>.

APPENDIX 3 - CODE

Motor Control

All motor control code is in the Arduino programming language for the Arduino Pro Mini. In terms of the shift register, outputs B-D were connected to the H-bridge inputs for coils 1-3 respectively and outputs E-G were connected to the H-bridge EN's for their respective coils. Thus, `sendByte(B01001000)`; energizes **coil 1** (not coil 2) in the “forward” direction. In reality, vis-à-vis Appendix 2, one might notice sending 1 from the shift encoder actually drives current in the “backwards” direction compared to the analysis circuit. Thus, if a positive p.d. is measured from the analysis circuit for a certain coil, a 1 should be pushed to the shift encoder of that coil to promote the forcer's velocity.

Global variables:

```
long last_micros = 0; //Timer
boolean flag = false; //Generic bit flag
```

Shift Encoder functions:

```
void sendBit(byte pack) {
  if(pack) {
    PORTD |= 1<<2; //Drive input SER pin high
    PORTD |= 1<<4; //Drive CLK pin high
    PORTD &= ~(1<<4); //Drive CLK pin low (falling-edge triggered)
  }
  else {
    PORTD &= ~(1<<2); //Drive input SER pin low
    PORTD |= 1<<4; //Drive CLK pin high
    PORTD &= ~(1<<4); //Drive CLK pin low (falling-edge triggered)
  }
}
void sendByte(byte pack) {
  for(byte i=0; i<8; i++) { //Loop through all bits in the byte
    //low end bit first, i.e. IN then ENABLE
    sendBit((pack>>i)&1);
  }
  latch(); //Latch serial buffer to parallel output
}
void latch() {
  PORTD |= 1<<3; //Drive latch (RCLK) pin high
  PORTD &= ~(1<<3); //Drive latch pin low (falling-edge triggered)
}
```

void setup() for all feedback code:

```
void setup() {
  for(byte i=0; i<14; i++) {
    pinMode(i, OUTPUT);
  }
  PORTB &= ~(B111); //All multiplexing FETs are driven low
  digitalWrite(11, HIGH); //Disable Serial CLR on shift register
  sendByte(B00100100); //Drive coil 2 forward (bits 2-4 set the direction, bits 5-7 are enable)
  delay(5000); //5000ms delay
  sendByte(B00011110); //IMPORTANT: asymmetrical config.; initial push in desired direction
  delayMicroseconds(10000); //10ms delay
}
```

3-COIL BRUSHLESS STYLE

```
if(micros()>last_micros+600) { //Do this every ~760us (600+100+3*20)
  sendByte(0); //Stop all current to coils
  delayMicroseconds(100); //Wait to reduce noise
  byte s = 0; //Recording byte
  for(byte i=0; i<3; i++) {
    byte port = PORTB;
    port &= ~(B111); //Disable all multiplexing FETs
    port |= 1<<i; //Enable the FET connected to the coil we want to analyze
    PORTB = port; //Set all pins at once: faster
    delayMicroseconds(20); //Wait 20us to reduce noise
    s<<=1; //Shift recording variable one bit left
    s|=digitalRead(15); //Append signage of feedback (1=positive, 0=negative)
  }
  sendByte(s<<4|B1110); //Send: recorded results as forward/backward flags for coils; enable all coils -
    to shift register
  last_micros = micros(); //Reset timer
}
```

2-COIL BRUSHLESS STYLE

```
if(!flag && micros()>last_micros+600) { //Do this every ~760us (600+100+3*20)
  sendByte(0); //Stop all current to coils
  delayMicroseconds(100); //Wait to reduce noise
  byte s = 0; //Recording byte
  boolean prev = false; //store previous sign of back EMF
  flag = false; //flag if more than one coil is to be energized
  signed int minimum = 1024; //minimum potential difference reading
  signed int maximum = -1024; //maximum potential difference reading
  byte m[2]; //coil numbers corresponding to minimum and maximum respectively
  for(byte i=0; i<3; i++) { //multiplex all coils
    byte port = PORTB; //store current digital output configurations
    port &= ~(B111); //disable all multiplexing FETs
    port |= 1<<i; //Enable the FET connected to the coil we want to analyze
    PORTB = port; //Set all pins at once: faster
    delayMicroseconds(20); //Wait 20us to reduce noise
    byte d = digitalRead(15); //Read sign of p.d. from coil we're analyzing
    signed int val = (d*2-1)*analogRead(0); //Apply sign of p.d. to absolute p.d. we read from amplifier
    if(i!=0 && d!=prev) { //If the sign is different from the previous one, we're using two coils
      flag = true;
    }
    else {
      prev = d; //set the "previous" sign to this one
    }
    if(val<minimum) { //If the measured p.d. is less than the minimum
      minimum = val; //set this to be the new minimum
      m[0] = 2-i; //set the minimum coil number to this one
    }
    if(val>maximum) { //same for maximum
      maximum = val;
      m[1] = 2-i;
    }
  }
  if(!flag) { //if the signs are all the same
    s=(prev<<(m[prev]+4))|(1<<(m[prev]+1)); //energize only the coil with the largest absolute p.d.
  }
  else {
    s=(1<<m[0]+1)|(B1001<<(m[1]+1)); //energize the two coils: maximum and minimum
  }
  sendByte(s); //Send to shift register
  last_micros = micros(); //Reset timer
}
```

1-COIL BRUSHLESS STYLE

```
if(!flag && micros()>last_micros+600) { //Do this every ~760us (600+100+3*20)
  sendByte(0); //Stop all current to coils
  delayMicroseconds(100); //Wait to reduce noise
  byte s = 0; //Recording byte
  byte m=0;
  boolean sgn = false; //Store sign of coil to be energized
```

```

signed int maximum = -1; //Store maximum absolute p.d. so far
for(byte i=0; i<3; i++) {
  byte port = PORTB; //store current digital output configurations
  port &= ~(B111); //disable all multiplexing FETs
  port |= 1<<i; //Enable the FET connected to the coil we want to analyze
  PORTB = port; //Set all pins at once: faster
  delayMicroseconds(20); //Wait 20us to reduce noise
  int val = analogRead(0); //Read absolute p.d.
  byte d = digitalRead(15); //Read sign of p.d. from coil we're analyzing
  if(val>maximum) { //If the absolute p.d. is the maximum
    maximum = val; //Set this value to be the new maximum
    m = 2-i; //Store the number of this coil
    sgn = d; //Record the sign of the coil
  }
}
s = (sgn<<(m+4))|(1<<(m+1)); //Activate only the coil with the greatest absolute p.d.
sendByte(s); //Send to shift register
last_micros = micros(); //Reset timer
}

```

Recording and Calculation

LOGGING SERIAL DATA (PYTHON)

```

import serial

ser = serial.Serial("/dev/tty.usbserial-A702LY8G", 115200)
f = open("/data_2.csv", "w")

vals = [0,0]

while True:
    try:
        line = ser.readline()
        f.write(line)
    except (KeyboardInterrupt, SystemExit):
        ser.close()
        f.close()

```

PROCESSING ALL DATA (PHP)

```

<?php
function doublemax($mylist){
  $maxvalue=max($mylist);
  while(list($key,$value)=each($mylist)){
    if($value==$maxvalue)$maxindex=$key;
  }
  return array("m"=>$maxvalue,"i"=>$maxindex);
}

$averages = array();
$z = 0;
$scanned_directory = array_diff(scandir($argv[1]), array('.', '..'));
foreach(array_reverse($scanned_directory) as $file) {
  if(preg_match("/trial(\d)\.csv/", $file, $matches)) {
    $z++;
    $e = explode("\n", str_replace("\n\n", "\n", file_get_contents($argv[1].$file)));
    $d = file_get_contents($argv[1].chr($matches[1]+96).".csv");
    $velocity = array();
    $acceleration = array();
    $position = array();
    $times = array();
    foreach(explode("\n", $d) as $k=>$line) {
      if($k==0) {
        continue;
      }
      list($t, $p, $v, $a) = explode(",", $line);
      array_push($position, $p); array_push($velocity, $v); array_push($acceleration,
$a); array_push($times, $t);
    }
    $flag = false;

```

```

foreach($e as $k=>$line) {
    list($current, $pd) = explode(",", $line);
    if($current>55) {
        $flag = true;
    }
    if($current<50 && $flag) {
        $pois = array();
        $pois_sum = array();
        $c = 0;
        foreach($velocity as $kd=>$d) {
            if($d>0) {
                if(empty($velocity[$kd-1]) || $velocity[$kd-1]<=0) {
                    $c++;
                    $pois[$c]=array();
                }
                $pois[$c][$kd]=$d;
                $pois_sum[$c]+=$d;
            }
        }
        $max = doublemax($pois_sum);
        $maxv = doublemax($pois[$max["i"]]);
        $time = sizeof($pois[$max["i"]])*0.02;
        $chunk = array_slice($e, $k, round($time*1468));
        $counter = 0;
        $c = 0;
        $p = 0;
        foreach($chunk as $val) {
            list($current, $pd) = explode(",", $val);
            if($current<200) {
                $c+=$current;
                $p+=$pd;
                $counter++;
            }
        }
        $powerin = (($p*10)/(1024*$counter))*(($c/(1024*$counter)*5)/0.4);
        echo "Potential difference: ".(($p*10)/(1024*$counter))."±".((1000/1024)/
(($p*10)/(1024*$counter)))."%\n";
        echo "Current: ".(($c/(1024*$counter)*5)/0.4)."±".((500/(0.4*1024))/((($c/
(1024*$counter)*5)/0.4)))."%\n";
        echo "Power In:". $powerin."|".($c/$counter)."\n";
        echo "Power out over time:\n";
        foreach($pois[$max["i"]] as $k=>$val) {
            echo ($val*$velocity[$k]*0.0280);
            echo "|";
            echo $val;
            echo "\n";
        }
        echo "Efficiency over time:\n";
        $div = array();
        $max_e = 0;
        foreach($pois[$max["i"]] as $k=>$val) {
            if((($val*$acceleration[$k]*0.028063)*100/$powerin)>$max_e) {
                $max_e = (($val*$acceleration[$k]*0.0280)*100/$powerin);
            }
            if(!empty($pois[$max["i"]][$k+1]) && $k!=0) {
                $div[$k]=((($pois[$max["i"]][$k+1]-$pois[$max["i"]
[$k-1])/0.04);
            }
        }
        echo "Maximum efficiency: ". $max_e."\n";
        $keys = array_keys($pois[$max["i"]]);
        echo "Energy Efficiency:". (0.028063*((pow($velocity[$maxv["i"]], 2)/2-
pow($velocity[$keys[0]], 2)/2)/$powerin)*1/((($maxv["i"]-$keys[0])*0.02))."\n";
        array_push($averages, (0.028063*((pow($velocity[$maxv["i"]], 2)/2-
pow($velocity[$keys[0]], 2)/2)/$powerin)*1/((($maxv["i"]-$keys[0])*0.02)));
        break;
    }
}
}
}
$mean = array_sum($averages)/sizeof($averages);
$u = 0;

```



```

foreach($averages as $a) {
    if(abs($a-$mean)>$u) {
        $u = abs($a-$mean);
    }
}
echo "Average Efficiency: ".$mean*100."±".$u*100."\n";
?>

```

APPENDIX 4 - GRAPHS AND SAMPLE DATA

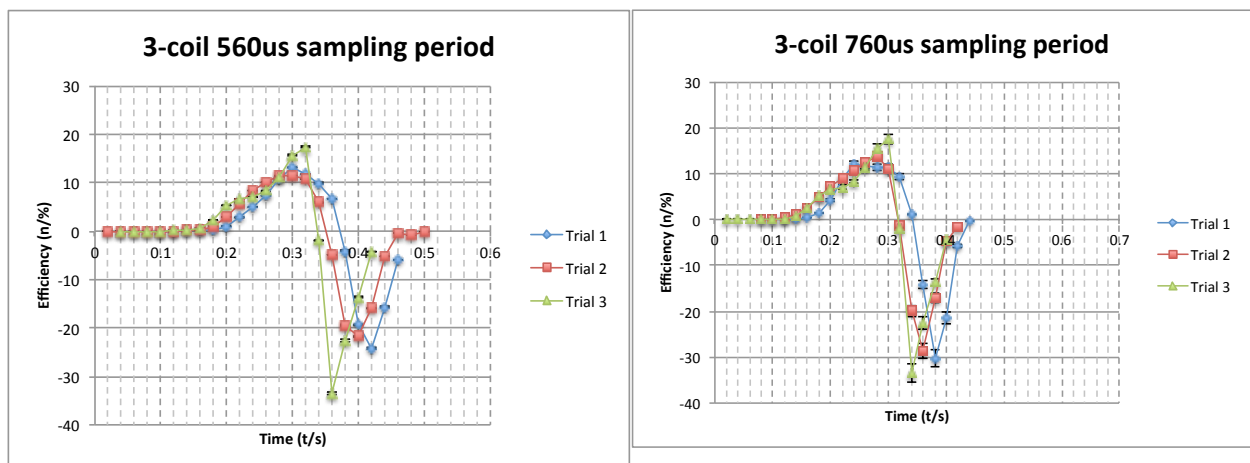
Sample raw data from ammeter and voltmeter ADC

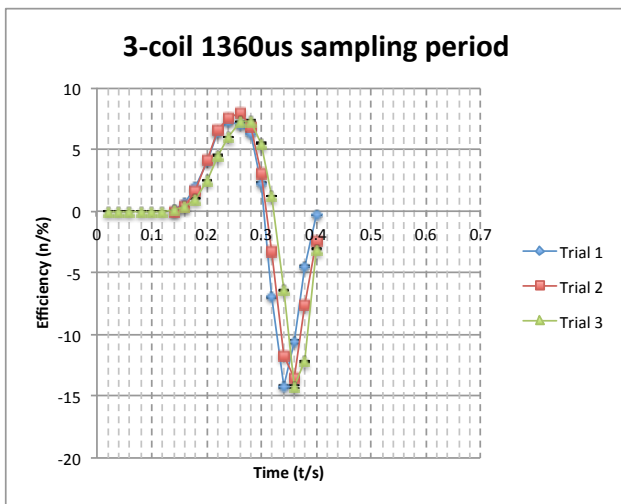
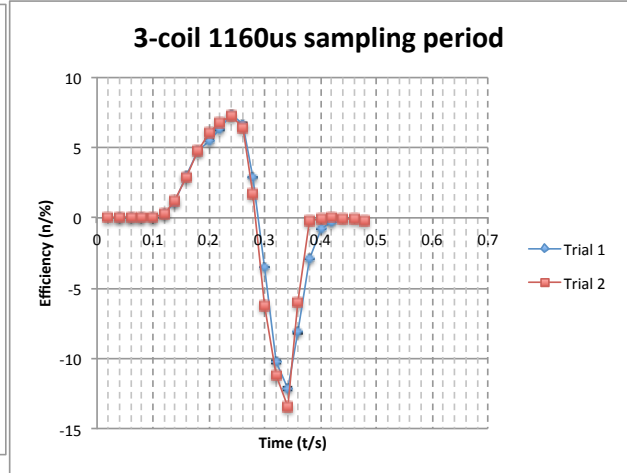
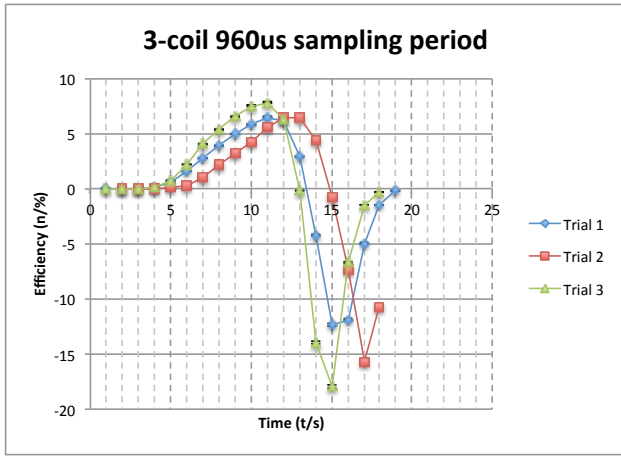
| Time (t/ μ s) | Current ADC reading | Potential Difference ADC reading |
|-------------------|---------------------|----------------------------------|
| 861±0.1 | 27±1 | 767±1 |
| 1722±0.1 | 21±1 | 772±1 |
| 2583±0.1 | 23±1 | 777±1 |
| 3444±0.1 | 17±1 | 767±1 |
| 4305±0.1 | 31±1 | 767±1 |
| 5166±0.1 | 20±1 | 771±1 |
| 6027±0.1 | 21±1 | 767±1 |
| 6888±0.1 | 17±1 | 756±1 |
| 7749±0.1 | 60±1 | 748±1 |
| 8610±0.1 | 59±1 | 748±1 |
| 9471±0.1 | 56±1 | 772±1 |
| 10332±0.1 | 60±1 | 747±1 |
| 11193±0.1 | 4±1 | 768±1 |
| 12054±0.1 | 60±1 | 746±1 |
| 12915±0.1 | 3±1 | 768±1 |
| 13776±0.1 | 61±1 | 747±1 |
| 14637±0.1 | 4±1 | 755±1 |
| 15498±0.1 | 61±1 | 747±1 |
| 16359±0.1 | 7±1 | 752±1 |
| 17220±0.1 | 60±1 | 747±1 |
| 18081±0.1 | 31±1 | 747±1 |

Sample table of power efficiency vs. acceleration, velocity, position and time for 2-coil sequence, sampling period = 760 μ s

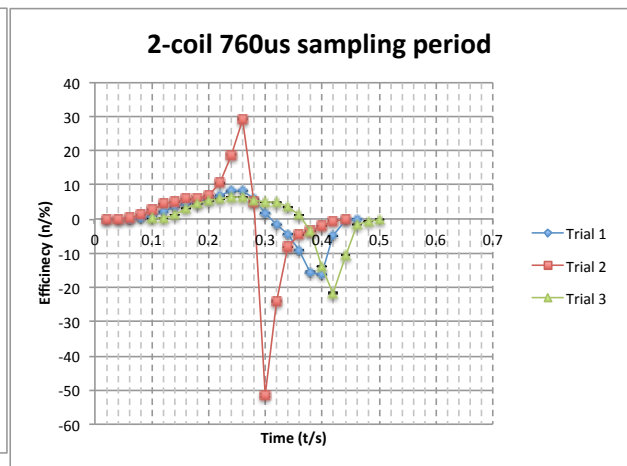
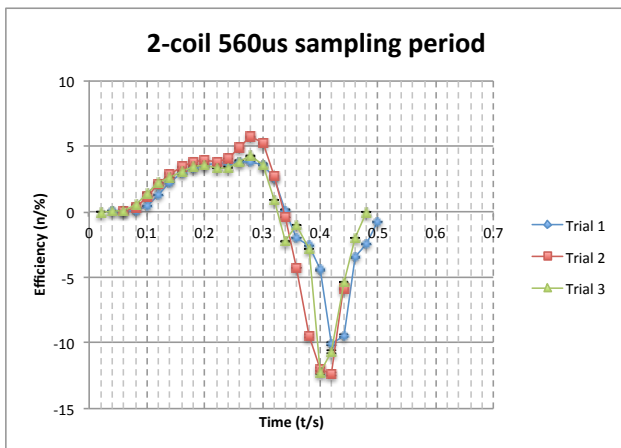
| Time (t/s) | Position (d/m $\pm 0.001\text{m}$) | Velocity (v/ $\text{m}\cdot\text{s}^{-1}$) | Acceleration (v/ $\text{m}\cdot\text{s}^{-2}$) | Efficiency ($\eta/\%$) |
|------------|--|--|---|--------------------------|
| 1.16 | 0.507 \pm 0.001 | 0.005 \pm 0.00002 | 1.268 \pm 0.0001 | 0.011 \pm 0.0008 |
| 1.18 | 0.507 \pm 0.001 | 0.035 \pm 0.0001 | 3.041 \pm 0.003 | 0.187 \pm 0.005 |
| 1.2 | 0.507 \pm 0.001 | 0.12 \pm 0.0005 | 5.062 \pm 0.004 | 1.067 \pm 0.01 |
| 1.22 | 0.51 \pm 0.001 | 0.252 \pm 0.001 | 6.3 \pm 0.004 | 2.788 \pm 0.02 |
| 1.24 | 0.517 \pm 0.001 | 0.401 \pm 0.002 | 6.1 \pm 0.004 | 4.296 \pm 0.02 |
| 1.26 | 0.528 \pm 0.001 | 0.501 \pm 0.002 | 5.487 \pm 0.004 | 4.828 \pm 0.03 |
| 1.28 | 0.537 \pm 0.001 | 0.608 \pm 0.002 | 5.316 \pm 0.004 | 5.676 \pm 0.03 |
| 1.3 | 0.552 \pm 0.001 | 0.724 \pm 0.003 | 4.816 \pm 0.004 | 6.123 \pm 0.03 |
| 1.32 | 0.567 \pm 0.001 | 0.799 \pm 0.003 | 4.717 \pm 0.004 | 6.619 \pm 0.04 |
| 1.34 | 0.583 \pm 0.001 | 0.878 \pm 0.003 | 6.742 \pm 0.01 | 10.396 \pm 0.1 |
| 1.36 | 0.602 \pm 0.001 | 1.015 \pm 0.003 | 10.54 \pm 0.01 | 18.788 \pm 0.1 |
| 1.38 | 0.621 \pm 0.001 | 1.283 \pm 0.004 | 12.918 \pm 0.01 | 29.106 \pm 0.02 |
| 1.4 | 0.644 \pm 0.001 | 1.835 \pm 0.006 | 1.517 \pm 0.0004 | 4.889 \pm 0.2 |
| 1.6 | 0.713 \pm 0.001 | 1.565 \pm 0.005 | -18.719 \pm 0.005 | -51.447 \pm 0.08 |
| 1.8 | 0.721 \pm 0.001 | 0.665 \pm 0.002 | -20.544 \pm 0.003 | -23.992 \pm 0.03 |
| 2.0 | 0.721 \pm 0.001 | 0.482 \pm 0.001 | -9.848 \pm 0.002 | -8.336 \pm 0.01 |
| 2.2 | 0.737 \pm 0.001 | 0.465 \pm 0.001 | -5.71 \pm 0.002 | -4.663 \pm 0.01 |
| 2.4 | 0.744 \pm 0.001 | 0.347 \pm 0.0009 | -5.883 \pm 0.002 | -3.585 \pm 0.006 |
| 2.6 | 0.751 \pm 0.001 | 0.198 \pm 0.0005 | -5.806 \pm 0.001 | -2.019 \pm 0.001 |
| 2.8 | 0.751 \pm 0.001 | 0.068 \pm 0.0002 | -3.899 \pm 0.0005 | -0.466 \pm 0.001 |

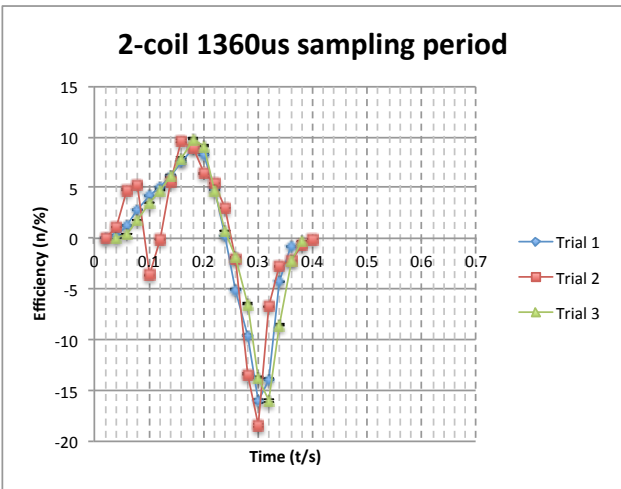
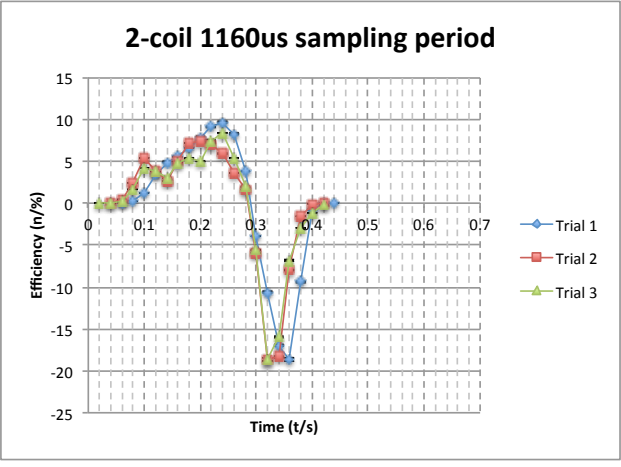
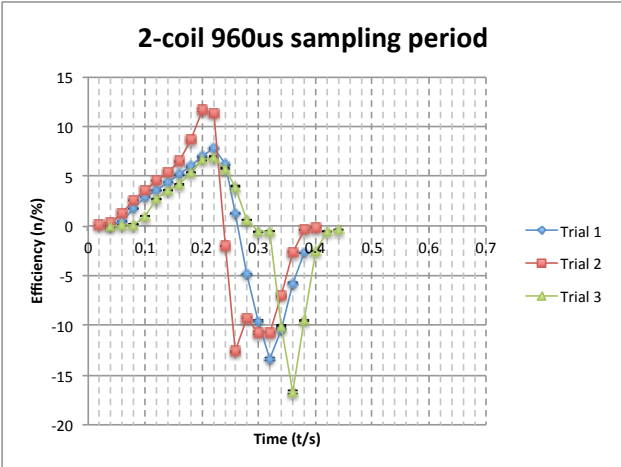
3-COIL SEQUENCE: DISCREPANCIES BETWEEN TRIALS



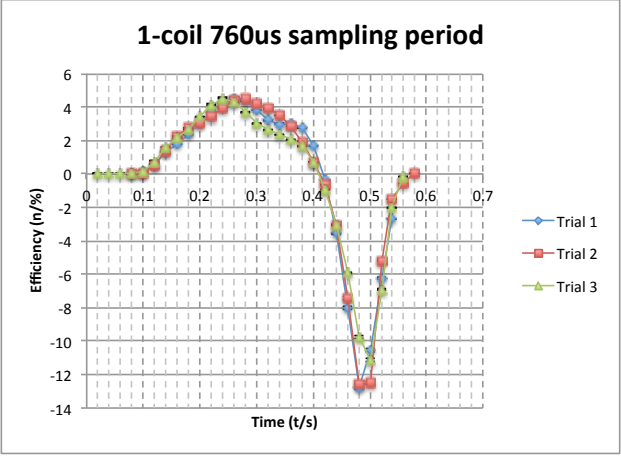
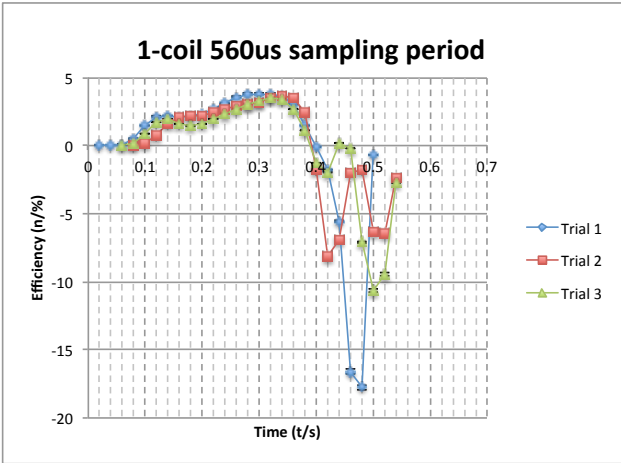


2-COIL SEQUENCE: DISCREPANCIES BETWEEN TRIALS

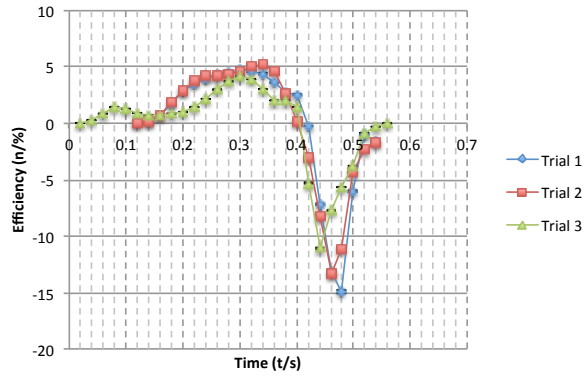




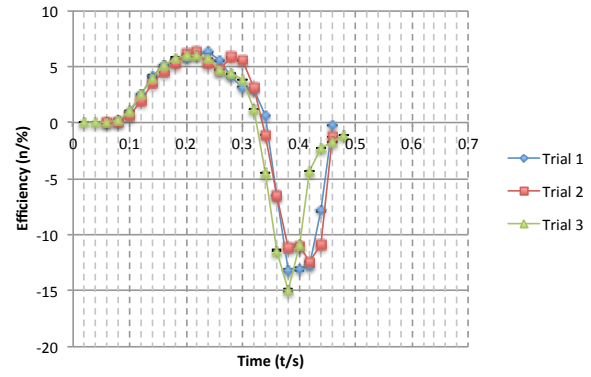
I-COIL SEQUENCE: DISCREPANCIES BETWEEN TRIALS



1-coil 960us sampling period



1-coil 1160us sampling period



1-coil 1360us sampling period

